Supporting Information for:

Long Range Proton-Coupled Electron Transfer Reactions of Bis(imidazole) Iron Tetraphenylporphyrins Linked to Benzoates

Jeffrey J. Warren,[a,b] Artur R. Menzeleev,[b] Joshua S. Kretchmer,[b]
Thomas F. Miller, III,[b]* Harry B. Gray[b]* and James M. Mayer[a]*

[a] *University of Washington, Department of Chemistry Seattle, WA 98195*
[b] *California Institute of Technology, Department of Chemistry, Pasadena, CA 91125*

mayer@chem.washington.edu, hbgray@caltech.edu, tfm@caltech.edu

Contents:

1. General S2

2. Synthesis of compounds S3

3. Electrochemistry S5

4. pK_a titrations S6

5. UV-Vis kinetics S7

6. Mechanism for Reaction $2^{(n)}$ S11

7. Estimates of the Fe···O distances S11

8. Details of the theoretical and computational analysis

8.1. Derivation of the CPET rate expression. S12

8.2. Molecular Dynamics Simulation Details S15

8.3. Calculation of $w_r^{(n)}(R)$ and $w_p^{(n)}(R)$ S22

8.4. Calculation of CPET Reorganization Energies S27

8.5. Calculation of $\Delta G^{o(n)}$ and $\Delta\Delta G^{o}$ S31

8.6. Decorrelation of the proton and electron donor-acceptor distances, and insensitivity of the proton donor-acceptor distance distribution to phenylene linker length S31

8.7. Molecular geometries S35

1. General

All solutions were prepared in a nitrogen filled glovebox unless otherwise noted. Reagents were purchased from Aldrich, with the exception of DBU (Strem). *N*-methylimidazole (MeIm) was purified by vacuum distillation, and was stored under an inert atmosphere. TEMPOH was synthesized from TEMPO$^{\bullet}$ following the literature procedure. [1] Tetrabutylammonium hexafluorophosphate ($^{n}Bu_4NPF_6$) was recrystallized 3 times from absolute ethanol, and dried in vacuo for 10 hours at 100 °C. DBU (1,8-diazabicyclo[5.4.0]undec-7-ene) was stored in a N_2-filled glovebox and used as received. Et_3N was freshly distilled from CaH_2, degassed and stored in a N_2-filled glovebox.

Solvents were purchased from Fischer and deuterated solvents were purchased from Cambridge Isotope Labs. Acetonitrile was used as received from Burdick and Jackson (low water) and was stored in an argon pressurized stainless steel drum, plumbed directly into a glovebox. Methylene chloride, diethyl ether, pentane, toluene and benzene were dried using a "Grubbs type" Seca Solvent System installed by GlassContour.[2]

Instrumentation ^{1}H NMR spectra were obtained on Bruker 300 or 500 MHz spectrometers at 298 K, unless otherwise noted. Chemical shifts are reported in ppm relative to TMS by referencing to residual solvent. UV/visible spectra were collected at ambient temperature using a Hewlett-Packard 8453 diode array spectrophotometer and are reported as λ_{max} in nm (ε, M^{-1} cm^{-1}). Cyclic voltammograms were collected using an E2 Epsilon electrochemical analyzer (Bioanalytical Systems). Kinetic runs were performed on an OLIS RSM-1000 stopped-flow spectrophotometer.

(1) Mader, E. A.; Davidson, E. R.; Mayer, J. M. *J. Am. Chem. Soc.* **2007**, *129*, 5153-5166 (and Supporting Information).

(2) http://www.glasscontour.com

2. Synthesis of compounds

General. The spectroscopy of the compounds discussed below is very similar to the previous report of iron tetraphenyl porphyrin model systems.[3] For example, the UV-Vis spectra of the ferric porphyrins are essentially identical, independent of the porphyrin ligand.

Fe^{III}(5-(4-carboxyphenyl)-10,15-20-triphenylporphyrin)Cl. The carboxyphenyl porphyrin was synthesized following the literature.[4] Iron was inserted following be refluxing with $Fe^{III}Cl_3$ in *N,N*-dimethylformamide.[5] However, the resulting metallated porphyrin was found to be soluble in methanol, precluding the final washing step. Instead, the complex was dried under vacuum, dissolved in methylene chloride and crystallized by addition of *n*-hexanes. ^{1}H NMR ($CDCl_3$, 500 MHz): d 81.2, 80.5 (br s, 8H), 14.6 (s, 1H), 13.4 (s, 4H), 12.5 (s, 1H), 12.2 (s 3H) 11.6 (s, 1H), 8.2 (s, 3H), 6.5 (s,3H) 5.2 (s, 3H) ppm. UV-Vis: 419 (114000), 510 (10500), 579 (2900), 656 (sh, 2300), 690 (2300). High Resolution Mass Spectrometry: m/z (M+) = 742.1776 (obs), 742.12445 (obs).

Fe^{III}5-(1,1'-biphenyl-4-carboxylic acid)-10,15,20-triphenylporphyrin)Cl. The ligand and the metallated porphyrin were prepared as described above. ^{1}H NMR ($CDCl_3$, 500 MHz): 81.2 (br s, 8H), 14.0 (s, 1H), 13.5 (s, 4H), 12.9 (s, 1H), 12.3 (s 3H) 9.0 (s, 2H), 8.5 (s, 2H), 8.1 (s, 1H), 6.9 (s, 2H), 6.4 (s, 4H), 5.0 (s, 3H) ppm. UV-Vis: 419 (112000), 510 (10000), 579 (2800), 656 (sh, 2400), 690 (2400). High-resolution mass spectrometry: m/z (M+) = 823.15867 (obs), 823.15566 (obs).

Fe^{III}(5-(4-carboxyphenyl)-10,15-20-triphenylporphyrin)bis(*N*-methylimidazole) hexafluorophosphate ($Fe^{III}PhCO_2H$) was synthesized flowing our previously reported procedure,[3] a modification of Valentine's original preparation.[6] ^{1}H NMR (CD_3CN, 500 MHz): d 18.62 (s, 6H), 8.56 (s, 2H), 6.88 (s, 2H), 6.60 (s, 2H), 6.48 (s, 3H) 6.50 (s, 2H), 6.28 (s 6H), 4.98 (s, 4H), 4.90 (s, 2H), -7.63 (s, 2H), -16.74 (s, 2H), -17.24 (s, 6H) ppm.

Fe^{III}5-(1,1'-biphenyl-4-carboxylic acid)-10,15,20-triphenylporphyrin)bis(*N*-methyl-imidazole) hexafluorophosphate ($Fe^{III}Ph_2CO_2H$) was synthesized as described above for **$Fe^{III}PhCO_2H$.** ^{1}H NMR (CD_3CN, 500 MHz): d 18.29 (s, 6H), 8.33 (s, 2H), 7.79 (s, 2H), 7.19 (s, 2H), 6.62 (s, 2H) 6.49 (s, 3H), 6.28 (s 6H), 6.30 (s, 6H), 5.08 (s, 2H), 4.99 (s, 6H), -7.46 (s, 2H), -16.60 (s, 6H), -16.81 (s, 2H) ppm. One set of imidazole C-H resonances (2H) is not observable.

The ferrous species Fe^{II}(5-(4-carboxyphenyl)-10,15-20-triphenylporphyrin)bis(*N*-methylimidazole) **($Fe^{II}PhCO_2H$)** and Fe^{II}5-(1,1'-biphenyl-4-carboxylic acid)-10,15,20-triphenyl–porphyrin)bis(*N*-methylimidazole) (**$Fe^{II}Ph_2CO_2H$)** were generated with addition of one equivalent of cobaltocene (Cp_2Co) to an acetonitrile solution of the corresponding ferrous

(3) Warren, J. J.; Mayer, J. M. *J. Am. Chem. Soc.* **2008**, *130*, 2774-2776.

(4) Forneli, A.; Planells, M.; Sarmentero, M. A.; Martinez-Ferrero, E.; O'Regan, B. C.; Ballester, P.; Palomares, E. *J. Mater. Chem.* **2008**, *18*, 1652-1658.

(5) Niño, M.; Giraldo, M. E.; Páez-Mozo, E. A. *J. Mol. Catal. A: Chem.* **2001**, *175*, 139-151.

(6) Quinn, R.; Nappa, M.; Valentine, J. S. *J. Am. Chem. Soc.* **1982**, *104*, 2588-2595.

complex. This reaction is fully reversible with the addition of one equivalent of the one electron oxidant tri(*p*-tolylaminium)PF_6.

The deprotonated ferric species Fe^{III}(5-(4-phenyl-carboxylate)-10,15-20-triphenylporphyrin)bis(*N*-methylimidazole) **($Fe^{III}PhCO_2^-$)** and Fe^{II}5-(1,1'-biphenyl-4-carboxylate)-10,15,20-triphenyl–porphyrin)bis(*N*-methylimidazole) **($Fe^{III}Ph_2CO_2^-$)** were generated with addition of the strong base 1,8-diaza(5.4.0)dicycloundecane (DBU). The UV-Vis spectral changes were fully reversible upon addition of one equivalent of strong acid (e.g. trifluoromethanesulfonic acid).

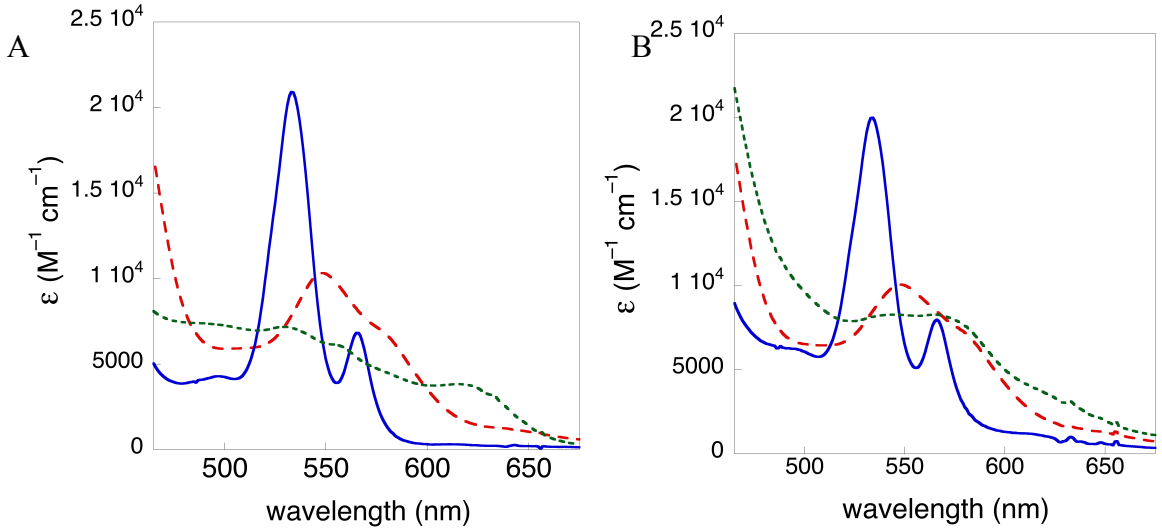

Figure S1. Visible spectra of the Q-bands of (A) **$Fe^{III/II}PhCO_2(H)$** species and (B) **$Fe^{III/II}Ph_2CO_2(H)$** species. In both (A) and (B) the solid blue line corresponds to the protonated ferrous compounds, the long dashed red line corresponds to the protonated ferric compounds and the short dashed green line corresponds to the deprotonated ferric compounds. The compounds represented by the solid and the short dashed lines differ formally by $H^\bullet$ ($H^+ + e^-$).

3. Electrochemistry.

The electrodes used were: working electrode, glassy carbon; reference electrode, $Ag^0/AgNO_3$ in electrolyte solution; and auxiliary electrode, platinum wire. All potentials are referenced versus internal ferrocene standard. The estimated errors are ±0.010 V. Scans were taken between 25 and 250 mV s^{-1} in the absence of ferrocene. The midpoint potential of the wave is not dependent upon scan rate. Ferrocene was added and cyclic voltammograms (CVs) were obtained at 25 and 100 mV s^{-1}. Addition of Cp_2Fe resulted in no change in peak potentials The ratio of peak currents is ~1 at all scan rates.

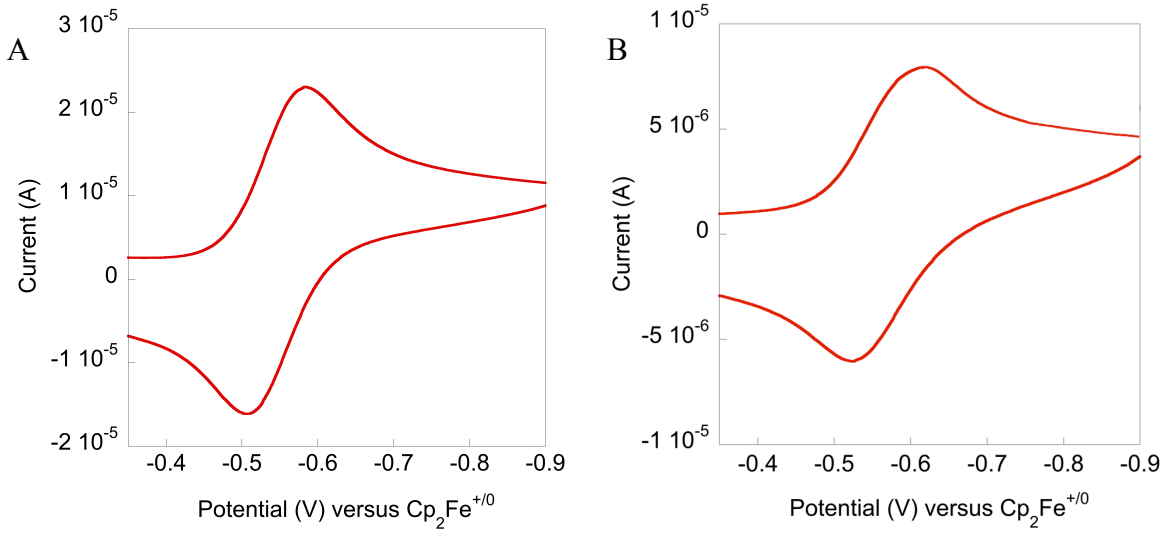

Figure S2. Cyclic voltammograms of *protonated* complexes (A) $\mathbf{Fe^{III/II}PhCO_2H}$ and (B) $\mathbf{Fe^{III/II}Ph_2CO_2^-}$. Glassy carbon working electrode, 100 mV/s.

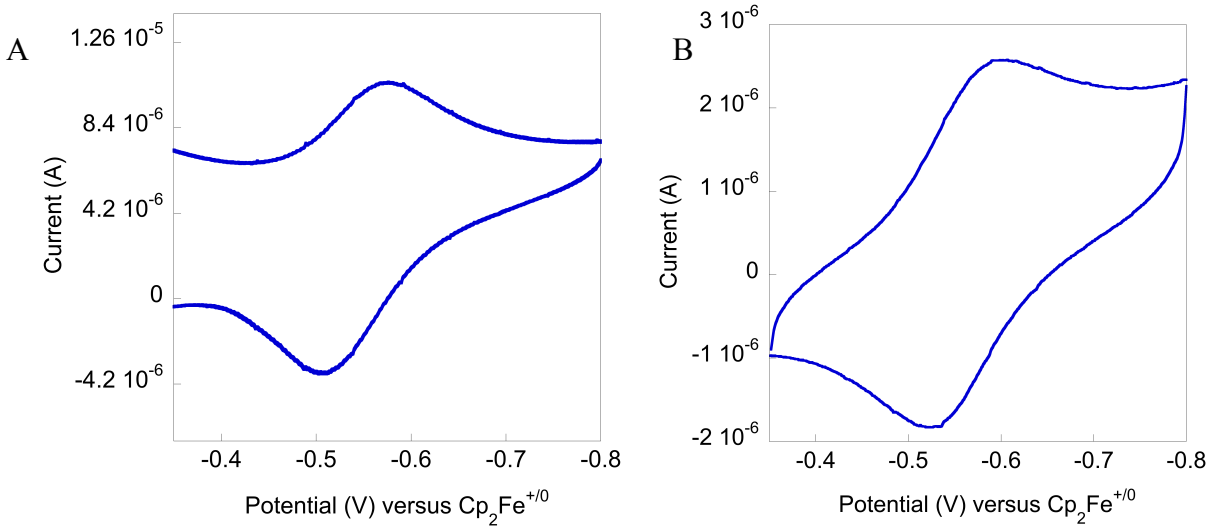

Figure S3. Cyclic voltammograms of **deprotonated** complexes (A) $\mathbf{Fe^{III/II}PhCO_2^-}$ and (B) $\mathbf{Fe^{III/II}Ph_2CO_2^-}$. Glassy carbon working electrode, 100 mV/s.

4. pK_a titrations.

All solutions were prepared under an inert atmosphere and used within 1 hour of preparation. Measurements were made at ambient temperature (295 K). Cuvettes were filled under an inert atmosphere and capped with a PTFE/Silicone coated septum (SpectroCell, USA). A fresh septum was used for each titration. Et_3N aliquots were added through the septum and data were immediately collected.

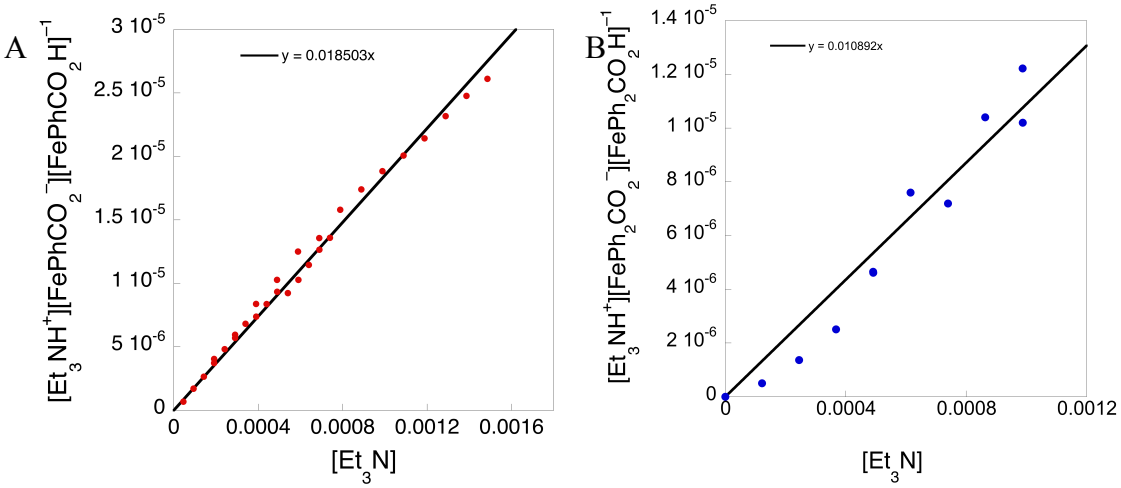

Figure S4. Mass balance plots for the titration of (A) **$Fe^{III}PhCO_2H$** and (B) **$Fe^{III}Ph_2CO_2H$** with Et_3N. The slope of the line gives the equilibrium constant for proton transfer between Et_3N and the respective porphyrin complex.

5. UV-Vis kinetics.

5.1 Stopped flow reactions.

All solutions used for kinetics were prepared in a N_2-filled glovebox. The stopped-flow syringes were loaded in the glovebox, and removed in pairs for each respective kinetic run. All measurements were at 298 K. All solutions of $\mathbf{Fe^{III}Ph_nCO_2^-}$ were freshly prepared from $\mathbf{Fe^{III}Ph_nCO_2H}$ + 1 equiv DBU immediately prior to use. These solutions were used immediately after mixing because $\mathbf{Fe^{III}Ph_nCO_2^-}$ has a tendency to precipitate, similar to a previous report.[7] Addition of stoichiometric acid regenerated the starting complex. All kinetics were performed in MeCN containing 0.1 ^{n}Bu$_4$NPF$_6$ + 5 mM MeIm, as previously described. Varying the starting concentration of iron starting material by up to a factor 3 for reactions 1 and 2 (main text) causes no change in the rate constants, indicating that they are first order in iron.

Reactions with TEMPOH were complicated by a side reaction that began after ~30-50% reaction; reactions could not be monitored over multiple half-lives, as is normally done. However, the initial rate of product formation (d[Fe^{II}]/dT) showed the same factor of 2 difference in rate constant ($k_{2,1}/k_{2,2}$) as described in the main text.

5.2 Other UV-Vis kinetics.

Reactions of $\mathbf{Fe^{III}Ph_nCO_2^-}$ with TEMPOH were too slow to be monitored by stopped-flow. Instead kinetic data were collected using a Hewlett Packard 8453 diode array spectrometer. All reaction solutions contained 0.1 ^{n}Bu$_4$NPF$_6$ + 5 mM MeIm in MeCN. Data were collected with continuous stirring and thermostated at 298 K.

All samples and solutions were prepared in a N_2-filled glove box. A screw-top quartz cuvette was charged with 3mL of a $\mathbf{Fe^{III}Ph_nCO_2H}$ solution. The cuvette was capped with a Teflon coated septum (fresh for each run) and removed from the glove box. Because the precipitation of the deprotonated ferric species was so problematic $\mathbf{Fe^{III}Ph_nCO_2^-}$ was generated by addition of 1 equivalent of DBU through the septum (addition of excess base greatly accelerated the precipitation reaction). Then, reactions were immediately initiated by addition of a solution of TEMPOH and monitored at regular intervals until the reactions were judged complete. The initial spectrum was often "missed" as reactions were initiated (as shown below). However, global analysis of reactions with and without these initial spectra was identical. The kinetics were also complicated by the extreme air sensitivity of the ferrous products, especially on the multiple minutes timescale of these experiments.

As for the stopped-flow reactions described above, a side reaction complicates the collection of kinetic data. This could be both precipitation and reaction of the ferrous products with O_2, or something else entirely. Working at lower (versus stopped-flow) iron and substrate concentrations largely ameliorates these problems, but kinetics traces still show some small deviations from ideal behavior (below). Changing the concentration of iron or TEMPOH does not change the observed rate constants and indicates that the reactions are first order in both iron and TEMPOH. Thus, the side reaction does not seem to strongly affect the observed rate constants.

---

(7) Warren, J. J.; Mayer, J. M. *J. Am. Chem. Soc.* **2011**, *133*, 8544-8551.

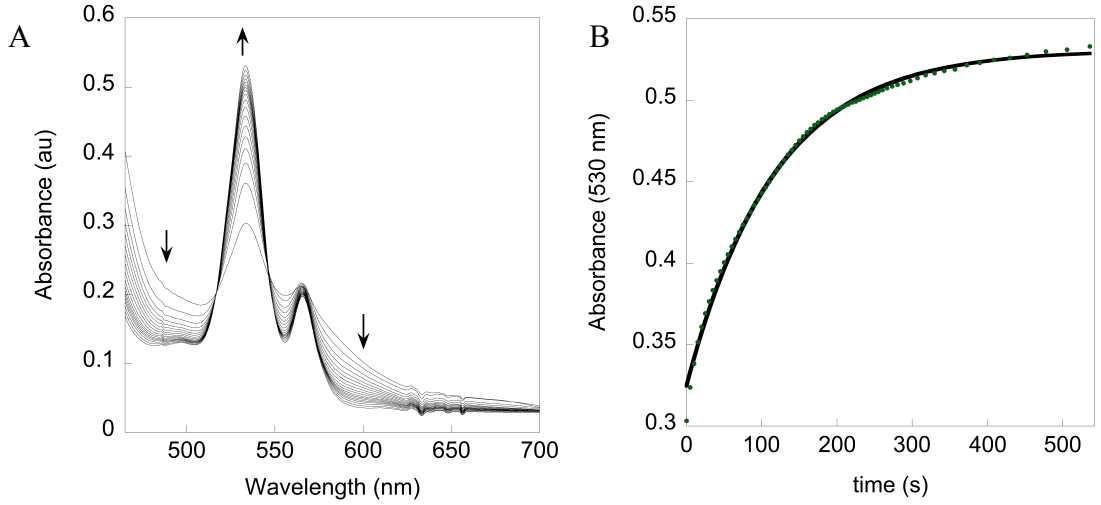

Figure S5. (A) Spectra and (B) trace at 530 nm for reaction of 1.1 10^{-3} M TEMPOH with 2.8 10^{-5} M mM **$FePhCO_2^-$**. The solid black line in (B) is a fit to a first order kinetics model.

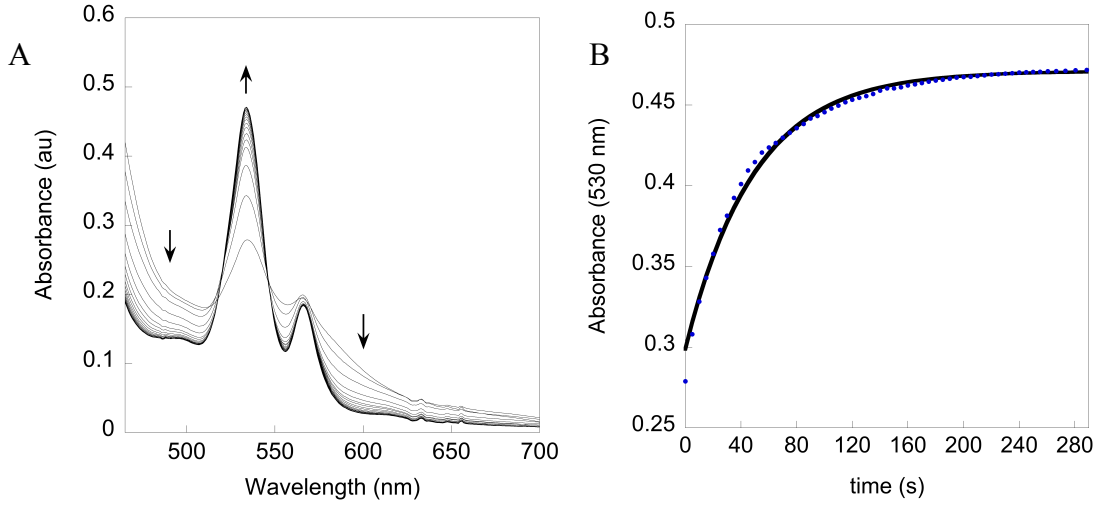

Figure S6. (A) Spectra and (B) trace at 530 nm for reaction of 3.75 10^{-3} M TEMPOH with 2.5 10^{-5} M **$FePh_2CO_2^-$**. The solid black line in (B) is a fit to a first order kinetics model.

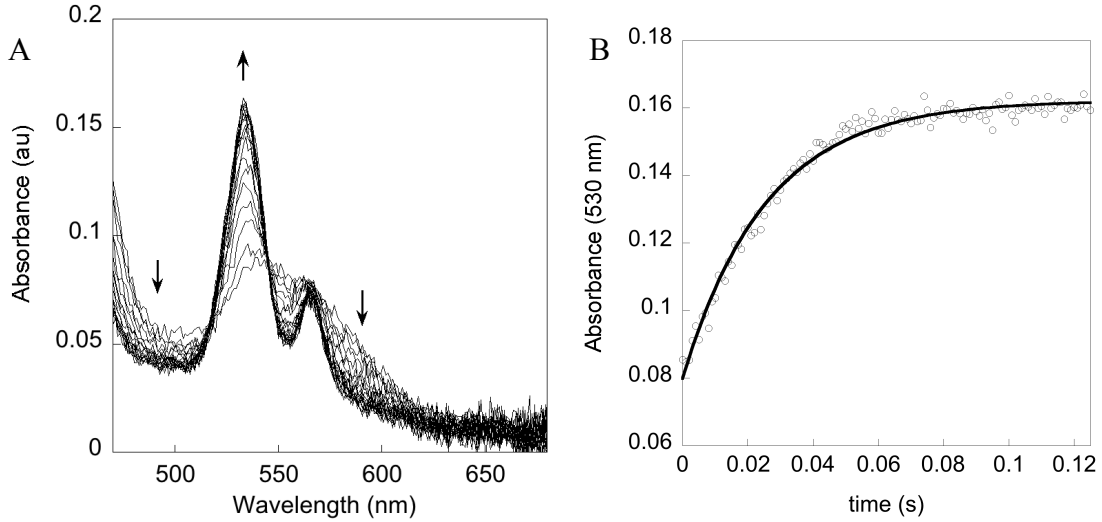

Figure S7. (A) Spectra and (B) trace at 530 nm for reaction of 7.5×10^{-5} M *i*AscH$^-$ with 7.5×10^{-6} M mM $\mathbf{FePh_2CO_2^-}$. The solid black line in (B) is a fit to a first order kinetics model.

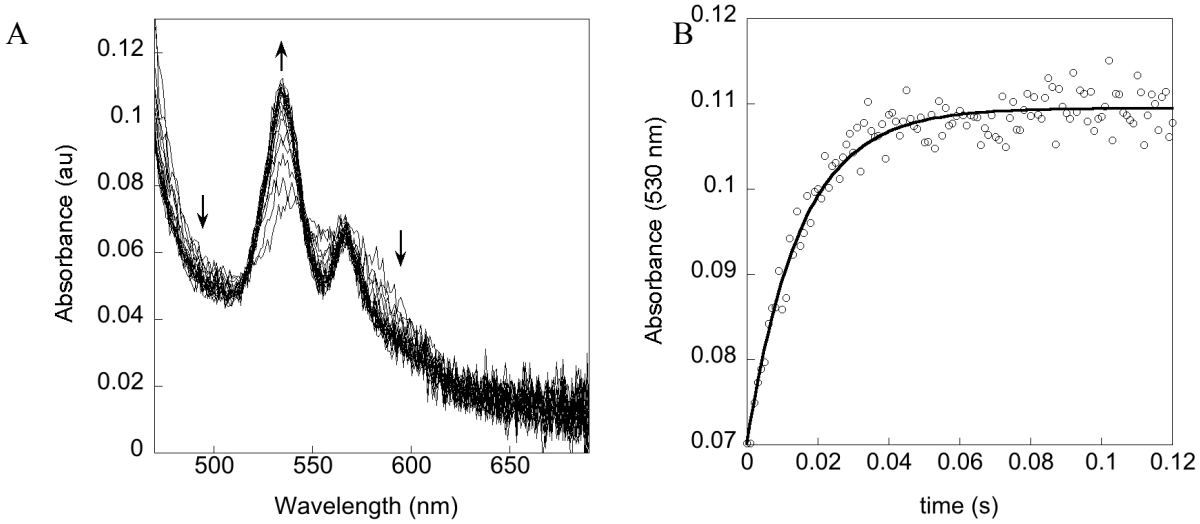

Figure S8. (A) Spectra and (B) trace at 530 nm for reaction of 8×10^{-5} M *i*AscH$^-$ with 8×10^{-6} M mM $\mathbf{FePh_2CO_2^-}$. The solid black line in (B) is a fit to a first order kinetics model.

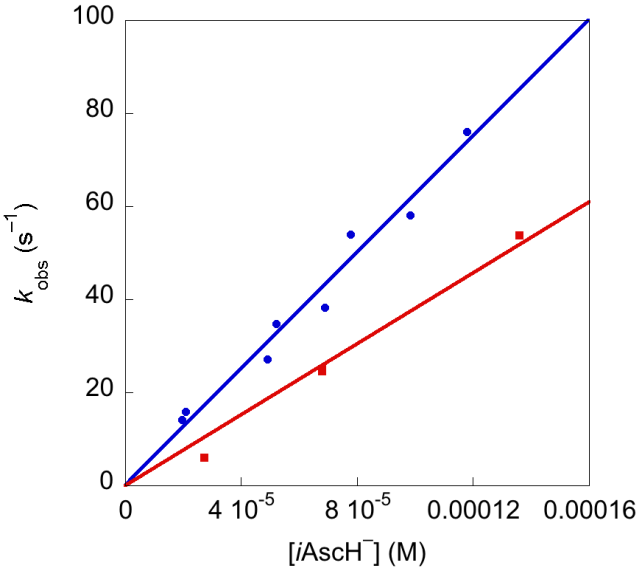

Figure S9. Plot of pseudo-first-order k_{obs} for reaction of $\mathbf{Fe^{III}PhCO_2^-}$ with *i*AscH$^-$ (blue ●) and *i*AscD$^-$ (red ■).

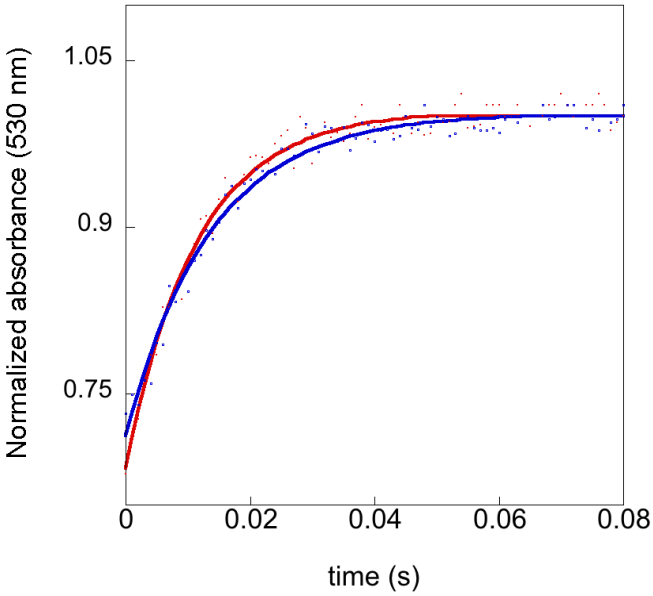

Figure S10. Example of the small KIE for $\mathbf{FePh_2CO_2^-}$ + iAscH(D)$^-$. Trace at 530 nm for reaction of 8 × 10^{-5} M $\mathbf{FePh_2CO_2^-}$ with 1.7 × 10^{-4} M *i*AscH$^-$ (red) and reaction of 9.1 × 10^{-5} M $\mathbf{FePh_2CO_2^-}$ with 1.7 × 10^{-4} M *i*AscD$^-$ The solid lines are fits to a first order kinetics model.

6. Mechanism of Reaction $2^{(n)}$

As noted in the main text, PCET reactions can occur via initial ET, initial PT or CPET. The ΔG^{o}_{PT} (8.6 kcal mol^{-1}) are near the observed Eyring barriers (9.5 and 9.6 kcal mol^{-1} for $2^{(1)}$ and $2^{(2)}$, respectively), making this path less likely. Analogous PT reactions have barriers in MeCN ($\Delta G^{\ddagger}_{PT} > \Delta G^{o}_{PT}$).[8]

Initial ET from *i*AscH^{-} to $\mathbf{Fe^{III}Ph_{\mathit{n}}CO_2^{-}}$, has ΔG^{o}_{ET}= 3.8 and 3.6 kcal mol^{-1}, for n = 1, 2 respectively. These are below the observed activation barriers (above). Initial ET cannot be ruled out. However, the observed kinetic isotope effects for are not consistent with rate limiting ET. Further, the free energy for CPET is much more favorable (ΔG^{o}_{CPET} = –3.9 kcal mol^{-1}) than that of initial ET. The mechanistic picture for $2^{(2)}$ is even less clear because of the very small KIE.

The kinetic behavior of Reaction 2 is similar to that of Reaction 1 where $k_x^{(1)} > k_x^{(2)}$ (x = Reaction 1 or 2). This observation is consistent with a PCET mechanism in which the bridge is important. If initial ET were operative, the bridge might not matter because *i*AscH^{-} could interact with the iron-porphyrin from any configuration, including those not involving the $(Ph)_n$ bridge.

7. Estimates of the Fe···O distances

The Fe···O distance in $\mathbf{Fe^{III}PhCO_2^{-}}$ was estimated from the reported structure of iron(III) tetra-4-carboxyphenylporphyrin chloride.[9] The same distance (9.9 Å) is obtained from adding the length of a carboxylate group to the 4-position of a phenyl ring in the bis(imidazole) complex of iron(III) tetraphenylporphyrin.[10]

The Fe···O distance in $\mathbf{Fe^{III}Ph_2CO_2^{-}}$ is estimated in the two ways described above, but two slightly different distances are obtained. An Fe···O distance of 14.0 Å is estimated from an x-ray structure of silver(II) substituted 5,10,15,20-tetrakis(4-carboxy-2,6-dimethylbiphenyl)-porphyrin, which is structurally similar to the iron complexes of 5-(1,1'-biphenyl-4-carboxylic acid)-10,15,20-triphenylporphyrin. Alternatively, by adding the length of a phenyl–CO_2H group to the structure of bis(imidazole) iron(III) tetraphenylporphyrin a distance of 14.2 Å is obtained. The consensus value is 14.1 Å.

(8) (a) Strohbusch, F.; Marshall, D.; Eyring, E. M. *J. Phys. Chem.* **1978**, *82*, 2447-2450. (b) Marshall, D. B.; Strohbusch, F.; Eyring, E. M. *J. Phys. Chem.* **1981**, *85*, 2270-2273.

(9) Schareina, T.; Kempe, R. *Z. Anorg. Allg. Chem.* **2000**, *626*, 1279-1281.

(10) Scheidt, W. R.; Osvath, S. R.; Lee, Y. J. *J. Am. Chem. Soc.* **1987**, *109*, 1958-1963.

8. Details of the theoretical and computational analysis.

A detailed derivation of the CPET rate equation (eq 3 in the main text) is presented in Section 8.1, and the computational model used for the MD simulation of CPET reactions $1^{(1)}$ and $1^{(2)}$ is described in Section 8.2. The subsequent sections describe the use of the model to calculate terms appearing in the CPET rate equation: Section 8.3 describes the calculation of the preorganization work terms, $w_{\mathrm{r}}^{(n)}(R)$ and $w_{\mathrm{p}}^{(n)}(R)$; Section 8.4 describes the calculation of the inner- and outer-sphere reorganization energies, $\lambda_{\mathrm{i}}^{(n)}(R)$ and $\lambda_{\mathrm{o}}^{(n)}(R)$; and Section 8.5 describes the calculation of the driving forces for reactions $1^{(1)}$ and $1^{(2)}$, $\Delta G^{o(1)}$ and $\Delta G^{o(2)}$, respectively. Finally, Section 8.6 describes the influence of the length of the linker domain on the proton donor-acceptor distance distributions, and Section 8.7 provides optimized molecular geometries.

8.1. Derivation of the CPET rate expression.

To describe the derivation and assumptions that yield eq 3 in the main text, we begin with the full expression for the bimolecular, electronically non-adiabatic CPET rate,[11]

$$k = \int dR \int dr \sum_j \sum_k \frac{2\pi}{\hbar} P_j \left|V_{jk}\right|^2 \left(4\pi\left(\lambda + \Delta\lambda_{jk}\right)k_{\mathrm{B}}T\right)^{-\frac{1}{2}} \times \exp\left[-\frac{\beta\left(\Delta G^{\circ} + \lambda + \Delta\lambda_{jk} + \epsilon_k - \epsilon_j\right)^2}{4\left(\lambda + \Delta\lambda_{jk}\right)}\right] \exp[-\beta w_{\mathrm{r}}], \tag{S1}$$

which explicitly includes the effect of conformational sampling in the electron and proton donor-acceptor distances, R and r, respectively. Here, j and k index the reactant and product vibrational states, respectively, P_j is the Boltzmann probability of the reactant vibrational state, V_{jk} is the CPET vibronic coupling, λ is the CPET reorganization energy for the ground vibrational sates, $\Delta\lambda_{jk}$ is the difference between the ground and excited vibrational state reorganization energies, ΔG° is the driving force for the CPET reaction, ϵ_j and ϵ_k are the respective energies of reactant and product vibrational states relative to their corresponding ground states, w_{r} is the work of preorganization for the reactants, and in this subsection $\beta = 1/(k_{\mathrm{B}}T)$. In general, each of these terms (aside from β) depends on both R and r. We suppress this dependence in the notation for the time being and will return to it shortly.

Defining a_{jk} and ϕ_{jk},

$$a_{jk} = \frac{2\pi}{\hbar} P_j |V_{jk}|^2 \left(4\pi\left(\lambda + \Delta_{jk}\right)k_B T\right)^{-\frac{1}{2}} \tag{S2}$$

$$\phi_{jk} = \Delta G^{\circ} + \Delta_{jk} + \epsilon_k - \epsilon_j \tag{S3}$$

eq S1 can be rewritten

(11) (a) Hammes-Schiffer, S.; Stuchebrukhov, A. A. *Chem. Rev.* **2010**, *110*, 6939. (b) Costentin, C.; Robert, M.; Saveant, J. M. *J. Am. Chem. Soc.* **2007**, *129*, 9953. (c) Cukier, R. I. *J. Phys. Chem.* **1995**, *99*, 16101.

$$k = \int dR \int dr \sum_j \sum_k a_{jk} \times \exp\left[-\beta\left(\frac{\lambda^2}{4(\lambda+\Delta_{jk})} + \frac{2\lambda\phi_{jk}}{4(\lambda+\Delta_{jk})} + \frac{\phi_{jk}^2}{4(\lambda+\Delta_{jk})}\right)\right] \exp[-\beta w_r]. \tag{S4}$$

This expression can be simplified upon noting that λ is large for the systems considered in this study (λ ≈40-45 kcal/mol, calculated in Section 8.4), whereas $\Delta\lambda_{jk} \sim 1$ kcal/mol. Therefore, to leading order, $\lambda + \Delta\lambda_{jk} \approx \lambda$,

$$a_{jk} = P_j |V_{jk}|^2 \sqrt{\frac{\pi}{\lambda k_B T\, \hbar^2}} \tag{S5}$$

and

$$k = \int dR \int dr \sum_j \sum_k a_{jk} \exp\left[-\beta\left(\frac{\lambda}{4} + \frac{\phi_{jk}}{2} + \frac{\phi_{jk}^2}{4\lambda}\right)\right] \exp[-\beta w_r]. \tag{S6}$$

We now argue that the term $\frac{\phi_{jk}^2}{4\lambda}$ can be neglected in eq S6. First, note that only the ground vibrational state of the reactant is thermally populated,

$$P_j = \begin{cases} 1, & j = 0 \\ 0, & j \neq 0 \end{cases} \tag{S7}$$

such that only terms associated with $j = 0$ in eq S6 need be considered. Furthermore, since ϵ_k is positive and increasing with k, the lowest value for ϕ_{0k} is $\phi_{00} = \Delta G°$, and ϕ_{0k} increases in the positive direction with k. It follows that since $\Delta G°$ is small in comparison to λ for the CPET reactions considered in this study ($\Delta G° \approx -3.5$ kcal/mol, calculated in Section 8.5), the term $\frac{\phi_{jk}^2}{4\lambda}$ is negligible for the $j = k = 0$ case, and $\frac{\phi_{0k}^2}{4\lambda}$ is only significant for values of k such that $\phi_{0k}/2 \sim \sqrt{\lambda}$. However, for such large values of ϕ_{0k}, the $\frac{\phi_{jk}}{2}$ term in the exponand of eq S6 truncates the sum with respect to k. The term $\frac{\phi_{jk}^2}{4\lambda}$ in eq S6 is thus indeed negligible for all j and k, and the rate expression simplifies to

$$k = \int dR \int dr \sum_j \sum_k a_{jk} \exp\left[-\beta\left(\frac{\lambda}{4} + \frac{\phi_{jk}}{2}\right)\right] \exp[-\beta w_r] \tag{S8}$$

$$= \int dR \int dr \left[\sum_j \sum_k P_j\, |V_{jk}|^2 \exp\left[-\beta\left(\frac{\Delta_{jk} + \epsilon_k - \epsilon_j}{2}\right)\right]\right] \times \sqrt{\frac{\pi}{\lambda k_B T \hbar^2}} \exp\left[-\beta\left(\frac{\lambda}{4} + \frac{\Delta G°}{2}\right)\right] \exp[-\beta w_r]. \tag{S9}$$

Next, we consider the degree to which the remaining terms in eq S9 are dependent upon coordinates r and R. For values of R that are sufficiently small that the TEMPOH-complex hydrogen bond is formed, Fig. S18 numerically demonstrates that the probability distributions for r and R are statistically uncorrelated. This lack of correlation, which will be invoked several times in the remainder of this subsection, follows from the fact that low-energy motions associated with changes in R, such as bending of the phenylene linker domain and rotations of

the TEMPOH molecule about the hydrogen bond, can occur without changes in r. Contributions to the CPET rate from configurations associated with larger values of R, for which the inter-complex hydrogen bond is dissociated, are negligible because they are thermally inaccessible in the preorganized reactant complex (i.e. the $e^{-\beta w_{\mathrm{r}}}$ term becomes relatively small in eq S9) and because the vibronic coupling becomes vanishingly small.

The terms P_j, $\Delta\lambda_{jk}$, ϵ_k, and ϵ_j are dependent upon the vibrational state of the transferring proton and are thus sensitive to the features of the hydrogen-bonding interface between $\mathbf{Fe^{III}Ph_nCO_2^-}$ and TEMPOH. The r-dependence of these terms is therefore included in this analysis. However, since changes in R do not significantly impact the hydrogen-bonding interface (Fig. S18), these terms are assumed to be independent of R.

As in previous studies, we neglect the dependence of λ on r.[12] This follows from the fact that fluctuations in r lead to relatively small changes in the charge distributions for either the reactant or product complexes. However, we do explicitly include the dependence of λ on R.

The preorganization work, w_{r}, accounts for both the work (along R) to bring the reacting species from infinite separation to a hydrogen-bonded configuration and the work (along r) necessary to compress the hydrogen bond to configurations that facilitate proton transfer. We thus explicitly include the dependence of both r and R in this term. Again using that the probability distributions for r and R are statistically uncorrelated for configurations that contribute to the CPET rate (Fig. S18), it follows that the joint probability distribution factorizes,

$$\rho(r,R) = \rho(r)\rho(R), \tag{S10}$$

such that the potential of mean force associated with these coordinates is additive,

$$w_{\mathrm{r}}(r,R) = w_{\mathrm{r}}(R) + w_{\mathrm{r}}(r). \tag{S11}$$

A similar arguments holds for the preorganization work for the products, $w_{\mathrm{p}}(r,R)$.

The driving force, $\Delta G°(r,R)$, for the CPET reaction at a particular value of r and R is given by[13]

$$\Delta G°(r,R) = \Delta G°_{\mathrm{CPET}} + w_{\mathrm{p}}(r,R) - w_{\mathrm{r}}(r,R), \tag{S12}$$

where $\Delta G°_{\mathrm{CPET}}$ is the driving force at infinite separation with respect to either r or R. The preceding analysis of $w_{\mathrm{r}}(r,R)$ and $w_{\mathrm{p}}(r,R)$ thus leads to an additive expression for the driving force,

$$\Delta G°(r,R) = \Delta G°(r) + \Delta G°(R). \tag{S13}$$

Lastly, note that in the regime of weak electronic coupling ($H_{AB} \ll k_{\mathrm{B}}T$), the CPET vibronic coupling takes the form[6,7,8]

$$V_{jk}(r,R) = \langle\, j \,|H_{\mathrm{AB}}(r,R)|\, k \,\rangle, \tag{S14}$$

where $H_{\mathrm{AB}}(r,R)$ is the electronic coupling matrix element, and $|j\rangle$ and $|k\rangle$ are the reactant and product vibrational wavefunctions, respectively. We then employ the standard Condon approximation that the electronic coupling is insensitive to changes in the proton position over the lengthscale of the proton vibrational wavefunctions, such that $H_{\mathrm{AB}}(r,R) = H_{\mathrm{AB}}(R)$, and[14]

---

(12) Edwards, J. S.; Soudackov, A. V.; Hammes-Schiffer, S. *J. Phys. Chem. A* **2009,** *113*, 2117.

(13) *cf.* (a) Marcus, R. A.; Sutin, N. *Biochim. Biophys. Acta* **1985**, *811*, 265. (b) Gray, H. B.; Winkler, J. R. *Biochim. Biophys. Acta* **2010**, *1797*, 1563. (c) Cordes, M.; Giese, B. *Chem. Soc. Rev.* **2009**, *38*, 892.

(14) (a) Hatcher, E.; Soudackov, A.; Hammes-Schiffer, S. *Chem. Phys.* **2005,** *319*, 93. (b) Ulstrup, J. *Charge Transfer Processes in Condensed Media*; Springer-Verlag: Berlin, 1979.(c) Cukier, R. I.; Nocera, D. G. *Annu. Rev. Phys. Chem.* **1998,** *49*, 337.

$$V_{jk}(r,R) = H_{\mathrm{AB}}(R)\langle\, j|k\,\rangle(r). \tag{S15}$$

Here, $\langle\, j|k\,\rangle(r)$ is the overlap between the reactant and product vibrational wavefunctions, which still strongly depends on r, and the electronic coupling preserves its dependence on R.

Inserting these results into eq S9 and separating the r- and R-dependent terms yields

$$\begin{aligned} k = \int dr \Bigg\{ & \sum_j \sum_k P_j(r)\, |\langle\, j|k\,\rangle(r)|^2 \\ & \times \exp\left[-\beta \left(\frac{\Delta\lambda_{jk}(r) + \epsilon_k(r) - \epsilon_j(r) + \Delta G^\circ(r)}{2} + w_{\mathrm{r}}(r) \right) \right] \Bigg\} \\ & \times \int dR\ |H_{\mathrm{AB}}(R)|^2 \sqrt{\frac{\pi}{\lambda(R) k_{\mathrm{B}} T \hbar^2}} \exp\left[-\beta \left(\frac{\lambda(R)}{4} + \frac{\Delta G^\circ(R)}{2} \right) \right] \mathrm{e}^{-\beta w_{\mathrm{r}}(R)} \end{aligned} \tag{S16}$$

$$= \gamma \int dR\, |H_{\mathrm{AB}}(R)|^2 \sqrt{\frac{\pi}{\lambda(R) k_{\mathrm{B}} T \hbar^2}} \exp\left[-\beta \left(\frac{\lambda(R)}{4} + \frac{\Delta G^\circ(R)}{2} \right) \right] \mathrm{e}^{-\beta w_{\mathrm{r}}(R)} \tag{S17}$$

which recovers eq 3 in the main text.

The analysis presented in this section employs approximations that are standard in the characterization of CPET reactions. The only novel aspect of this analysis is utilization of the fact that the coordinates r and R are statistically uncorrelated for configurations that contribute to the CPET rate, which is numerically demonstrated in Fig. S18.

8.2. Molecular Dynamics Simulation Details.

Molecular dynamics (MD) simulations of the PCET reactants employ a system comprised of $\mathbf{Fe^{III}PhCO_2^-}$, $\mathbf{Fe^{III}Ph_2CO_2^-}$, and a single TEMPOH molecule; simulations of the products employ a system comprised of $\mathbf{Fe^{II}PhCO_2H}$, $\mathbf{Fe^{II}Ph_2CO_2H}$, and a single TEMPO molecule. In both cases, the system also includes 2225 acetonitrile molecules and is performed in a 46.8 Å × 91.2 Å × 46.8 Å rectangular unit cell that is subject to periodic boundary conditions.

The porphyrin molecules, axial ligands, and TEMPOH/TEMPO molecules are modeled using the Generalized Amber Force Field (GAFF),[15] which is implemented using the DLPOLY molecular dynamics package.[16] The iron atom in both oxidation states is modeled using the Giammona parameters, which are included as the *frcmod.hemall* contributed parameter set for AMBER.[17] Atom-type assignment (Tables S1-3) is performed using the Antechamber program.[18] Acetonitrile molecules are represented with the three-site model of Guardia *et. al*.,[19] in which the

---

(15) Wang, J. M.; Wolf, R. M.; Caldwell, J. W.; Kollman, P. A.; Case, D. A. *J. Comput. Chem.* **2004,** *25*, 1157.
(16) Smith, W.; Forester, T. R. *J. Mol. Graph.* **1996,** *14*, 136.
(17) (a) Giammona, D. A. Ph.D thesis, University of California, Davis, **1984.** (b) Accessed at http://pharmacy.man.ac.uk/amber/.
(18) Wang, J.; Wang, W.; Kollman P. A.; Case, D. A. *J. Mol. Graph. Model.* **2006**, *25*, 247260.
(19) Guardia, E.; Pinzon, R.; Casulleras, J.; Orozco, M.; Luque, F. J. *Mol. Simulat.* **2001,** *26*, 287.

methyl group is represented as a single particle. In all calculations, the *N*-methylimidazole axial ligands are replaced by imidazole ligands.

In all MD simulations, short-range interactions are truncated at r_{cut} = 12 Å, and force-shifting[20] is employed for the truncation of long-range electrostatic interactions. Trajectories are thermostatted at a temperature of 298 K by resampling all atomic velocities from the Boltzmann distribution every 50 ps, and a timestep of 0.25 fs is employed to ensure accurate integration of the bond-stretching modes.

The charge distributions on the iron porphyrin complexes and the TEMPO/TEMPOH molecules are determined using density functional theory (DFT) calculations, performed using Gaussian 09 (version G09RevB.01).[21] For each species, the molecular geometry is optimized at the B3LYP/6-31G(d,p) level of theory. Solvation effects in these DFT calculations are included using the integral equation formalism of the polarizable continuum model,[22] with the default parameter values of the implementation in Gaussian 09.[23] The solute cavity is assembled from atom-centered spheres with radii corresponding to the atomic radii in the Universal Force Field (UFF) scaled by 1.1. The cavity surface is smoothly represented using the GePol-YK scheme,[24] and the acetonitrile static and optical dielectric constants have values of ε_o=35.688 and ε_∞=1.806874, respectively. Atomic point charges (Tables S1-S3) are determined by fitting the electrostatic potential from the electronic structure calculations using CHelpG (CHarges from Electrostatic Potentials using a Grid based method);[25] the charges for all atoms of the same atom-type are set to the mean value obtained from the CHelpG calculation.

In all MD simulations, the TEMPOH and TEMPO molecules are kept rigid at geometries that are optimized at the B3LYP/6-31G(d,p) level of theory; both molecules are most stable in the chair conformation with the oxygen atom in the equatorial position, and the OH torsion in TEMPOH assumes the *anti* conformation with respect to the axial methyl groups. The metalated porphyrin ring, the *meso*- substituents, and the axial ligands are also held rigid at the optimal geometry obtained at the B3LYP/6-31G(d,p) level, while the phenylene linker regions are left

---

(20) Brooks, C. L.; Pettitt, B. M.; Karplus, M. *J. Chem. Phys*. **1985,** *83*, 5897.
(21) Frisch, M. J.; Trucks, G. W.; Schlegel, H. B.; Scuseria, G. E.; Robb, M. A.; Cheeseman, J. R.; Scalmani, G.; Barone, V.; Mennucci, B.; Petersson, G. A.; Nakatsuji, H.; Caricato, M.; Li, X.; Hratchian, H. P.; Izmaylov, A. F.; Bloino, J.; Zheng, G.; Sonnenberg, J. L.; Hada, M.; Ehara, M.; Toyota, K.; Fukuda, R.; Hasegawa, J.; Ishida, M.; Nakajima, T.; Honda, Y.; Kitao, O.; Nakai, H.; Vreven, T.; Montgomery, Jr., J. A.; Peralta, J. E.; Ogliaro, F.; Bearpark, M.; Heyd, J. J.; Brothers, E.; Kudin, K. N.; Staroverov, V. N.; Kobayashi, R.; Normand, J.; Raghavachari, K.; Rendell, A.; Burant, J. C.; Iyengar, S. S.; Tomasi, J.; Cossi, M.; Rega, N.; Millam, N. J.; Klene, M.; Knox, J. E.; Cross, J. B.; Bakken, V.; Adamo, C.; Jaramillo, J.; Gomperts, R.; Stratmann, R. E.; Yazyev, O.; Austin, A. J.; Cammi, R.; Pomelli, C.; Ochterski, J. W.; Martin, R. L.; Morokuma, K.; Zakrzewski, V. G.; Voth, G. A.; Salvador, P.; Dannenberg, J. J.; Dapprich, S.; Daniels, A. D.; Farkas, Ö.; Foresman, J. B.; Ortiz, J. V.; Cioslowski, J.; Fox, D. J. *Gaussian 09,* Revision B.01; Gaussian, Inc.: Wallingford, CT, 2009.
(22) (a) Tomasi, J.; Mennucci, B.; Cancès, E.; *J. Mol. Struct. (Theochem)* **1999,** *464*, 211. (b) Tomasi, J.; Mennucci, B; Cammi, R. *Chem. Rev.* **2005**, *105*, 2999.
(21) Scalmani,G.; Frisch, M. J. *J. Chem. Phys.* **2010**, *132,* 114110.
(22) Pascual-Ahuir, J; Silla, E.; Tunon, I. *J. Comput. Chem*. **1994,** *15*, 1127.
(25) Breneman, C. M.; Wiberg, K. B. *J. Comput. Chem.* **1990,** *11*, 361.

unrestrained. The NOSQUISH algorithm[26] is employed to integrate the rigid-body equations of motion in the MD simulations. The optimized molecular geometries of TEMPO, TEMPOH, **$Fe^{III}PhCO_2^-$, $Fe^{II}PhCO_2H$, $Fe^{III}Ph_2CO_2^-$,** and **$Fe^{II}Ph_2CO_2H$,** are included in Tables S4-9 (Section 8.7).

We note that the MD force field employed here does not include electronic polarizability, which can significantly impact free energy calculations such as those reported here;[27] nonetheless, it can be expected that this effect is reduced upon consideration of relative free energies, such as those that appear in the determination of β (eqs. 6-8 in the main text).

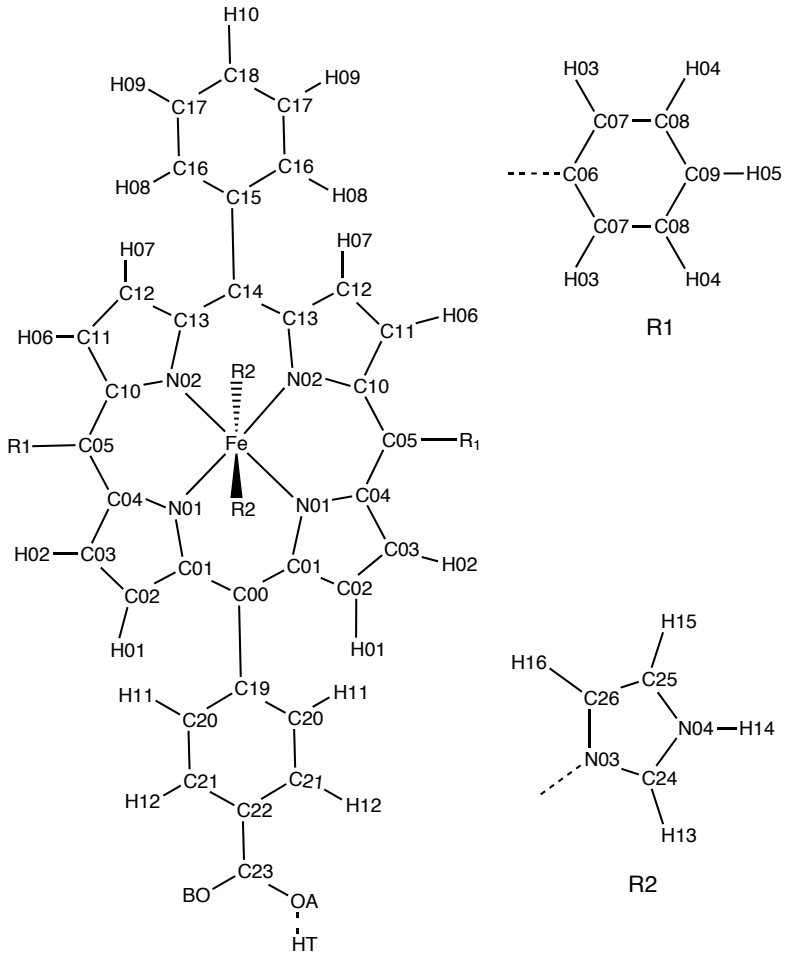

Figure S11. Atom types for the n=1 iron-porphyrin complex. R1 and R2 denote the phenyl substituents on the porphyrin ring and the axial imidazole ligands, respectively.

(26) Miller, T.F.; Eleftheriou, M.; Pattnaik, P.; Ndirango, A.; Newns, D.; Martyna, G. J. *J. Chem. Phys.* **2002,** *116*, 8649.

(27) (a) Zhao, X.G.; Cukier, R.I. *J. Phys. Chem.* **1995,** *99*, 945. (b) Gupta S.; Matyushov, D.M. *J. Phys. Chem. A* **2004,** *108*, 2087. (c) Vladimirov, E.; Ivanova, A.; and Rösch, N. *J. Chem. Phys.* **2008,** *129,* 194515.

Table S1. Atom types and charges in the reactant and product states for the *n*=1 iron porphyrin complex.

Atom Type	GAFF Atom Type	Reactant Charge	Product Charge
C00	cp	-0.030	-0.090
C01	cc/cd	0.082	0.069
C02	cc/cd	-0.086	-0.119
C03	cc/cd	-0.228	-0.258
C04	cc/cd	0.250	0.242
C05	cp	-0.144	-0.158
C06	cp	0.226	0.240
C07	ca	-0.192	-0.200
C08	ca	-0.059	-0.061
C09	ca	-0.125	-0.137
C10	cc/cd	0.237	0.233
C11	cc/cd	-0.214	-0.255
C12	cc/cd	-0.099	-0.113
C13	cc/cd	0.107	0.078
C14	cp	-0.080	-0.102
C15	cp	0.174	0.195
C16	ca	-0.133	-0.137
C17	ca	-0.068	-0.073
C18	ca	-0.143	-0.153
C19	cp	0.137	0.198
C20	ca	-0.145	-0.134
C21	ca	-0.089	-0.078
C22	ca	-0.075	-0.095
C23	c	0.682	0.672
C24	cc/cd	0.139	0.130
C25	cc/cd	-0.116	-0.145
C26	cc/cd	-0.005	0.014
Fe	Fe	0.731	0.602
H01	ha	0.097	0.088
H02	ha	0.118	0.108
H03	ha	0.116	0.113
H04	ha	0.099	0.095
H05	ha	0.106	0.105
H06	ha	0.115	0.107
H07	ha	0.095	0.079
H08	ha	0.076	0.071
H09	ha	0.104	0.102
H10	ha	0.113	0.110
H11	ha	0.073	0.081
H12	ha	0.089	0.119
H13	ha	0.060	0.042
H14	ha	0.366	0.356
H15	ha	0.179	0.170
H16	ha	0.063	0.038
N01	nd	-0.287	-0.276
N02	nd	-0.292	-0.278
N03	nd	-0.251	-0.277
N04	na	-0.233	-0.242
OA	o*	-0.749	-0.590
OB	o	-0.749	-0.570
HT	ho	—	0.445

* Atom type of OA is set to **oh** in the simulations of the product species.

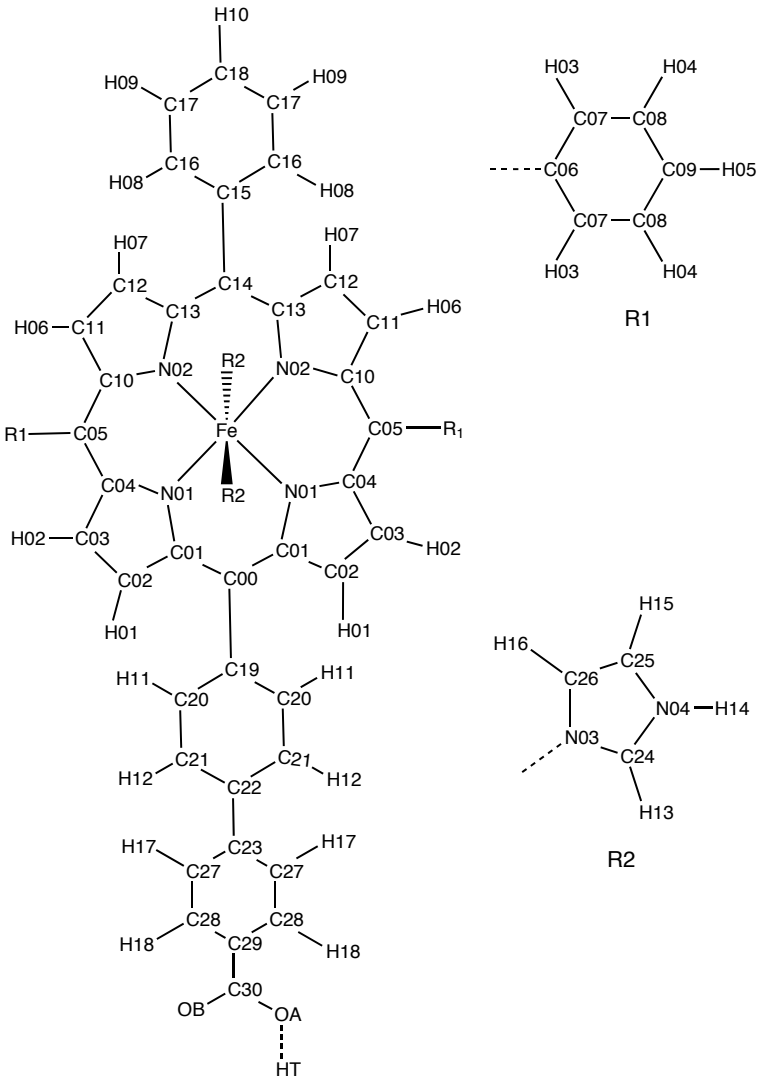

Figure S12. Atom types for the *n*=2 iron-porphyrin complex. R1 and R2 denote the phenyl substituents on the porphyrin ring and the axial imidazole ligands, respectively.

Table S2. Atom types and charges in the reactant and product states for the *n*=2 iron porphyrin complex.

Atom Type	GAFF Atom Type	Reactant Charge	Product Charge
C00	cp	-0.053	-0.102
C01	cc/cd	0.066	0.066
C02	cc/cd	-0.068	-0.098
C03	cc/cd	-0.223	-0.262
C04	cc/cd	0.217	0.239
C05	cp	-0.131	-0.154
C06	cp	0.211	0.231
C07	ca	-0.186	-0.197
C08	ca	-0.062	-0.064
C09	ca	-0.117	-0.127
C10	cc/cd	0.230	0.232
C11	cc/cd	-0.214	-0.258
C12	cc/cd	-0.094	-0.105
C13	cc/cd	0.087	0.074
C14	cp	-0.067	-0.105
C15	cp	0.206	0.193
C16	ca	-0.158	-0.132
C17	ca	-0.062	-0.086
C18	ca	-0.138	-0.129
C19	cp	0.147	0.184
C20	ca	-0.123	-0.127
C21	ca	-0.114	-0.109
C22	cp	0.025	-0.010
C23	cp	0.053	0.123
C24	cc/cd	0.121	0.150
C25	cc/cd	-0.106	-0.140
C26	cc/cd	-0.015	0.028
C27	ca	-0.141	-0.147
C28	ca	-0.099	-0.074
C29	ca	-0.044	-0.063
C30	c	0.656	0.645
Fe	Fe	0.818	0.677
H01	ha	0.083	0.073
H02	ha	0.119	0.107
H03	ha	0.114	0.114
H04	ha	0.100	0.095
H05	ha	0.104	0.101
H06	ha	0.116	0.107
H07	ha	0.093	0.076
H08	ha	0.082	0.070
H09	ha	0.104	0.104
H10	ha	0.108	0.102
H11	ha	0.083	0.080
H12	ha	0.105	0.107
H13	ha	0.070	0.036
H14	ha	0.359	0.358
H15	ha	0.175	0.169
H16	ha	0.069	0.029
H17	ha	0.086	0.102
H18	ha	0.082	0.112
N01	nd	-0.254	-0.284
N02	nd	-0.277	-0.284
N03	nd	-0.298	-0.310
N04	na	-0.211	-0.253
OA	o*	-0.744	-0.584
OB	o	-0.744	-0.563
HT	ho	—	0.444

* Atom type of OA is set to **oh** in the simulations of the product species.

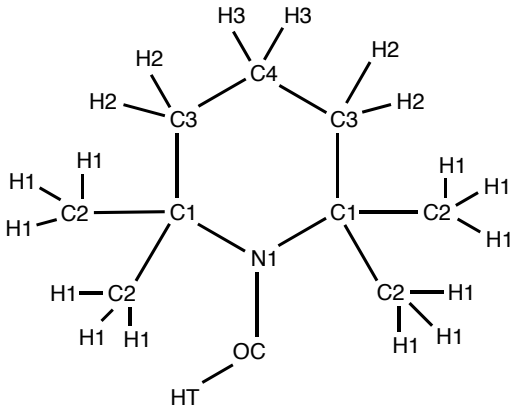

Figure S13. Atom labels for the TEMPOH molecule.

Table S3. TEMPOH atom types and charges in the reactant and product states.

Atom Type	GAFF Atom Type	Reactant Charge	Product Charge
C1	c3	0.800	0.518
C2	c3	-0.306	-0.287
C3	c3	-0.319	-0.262
C4	c3	0.198	0.094
N1	n	-0.730	-0.117
H1	hc	0.057	0.068
H2	hc	0.050	0.060
H3	hc	-0.027	0.005
OC	oh*	-0.492	-0.407
HT	ho	0.451	—

* Atom type of OC is set to **o** in the simulations of the product species

8.3. Calculation of $w_{\mathrm{r}}^{(n)}(R)$ and $w_{\mathrm{p}}^{(n)}(R)$.

Here, we describe the MD simulations that are used to calculate the reactant and product free energy profiles as a function of the electron donor-acceptor distance, $w_{\mathrm{r}}^{(n)}(R)$ and $w_{\mathrm{p}}^{(n)}(R)$, respectively. To robustly and efficiently obtain the relative free-energy profiles for the shorter (n=1) phenylene linker relative to the corresponding profiles for the longer (n=2) linker, some care must be taken in the design of the simulation protocol, as is now described.

Fig. S14 presents the simulation setup that is employed for the calculation of the reactant free energy profiles, $w_{\mathrm{r}}^{(1)}(R)$ and $w_{\mathrm{r}}^{(2)}(R)$. The $\mathbf{Fe^{III}PhCO_2^-}$ and $\mathbf{Fe^{III}Ph_2CO_2^-}$ molecules are arranged such that the distance between the iron centers is large (49.1 Å) and the linker region of each porphyrin is oriented toward the other along the y-axis (detailed geometries provided in Table S11). The rigid portions of the iron-porphyrin molecules (*i.e.*, the metalated porphyrin ring, the *meso*- substituents, and the axial ligands) are kept fixed in absolute space during all MD simulations. An analogous simulation setup is used to compute the free-energy profiles for the product species (detailed geometries provided in Table S12).

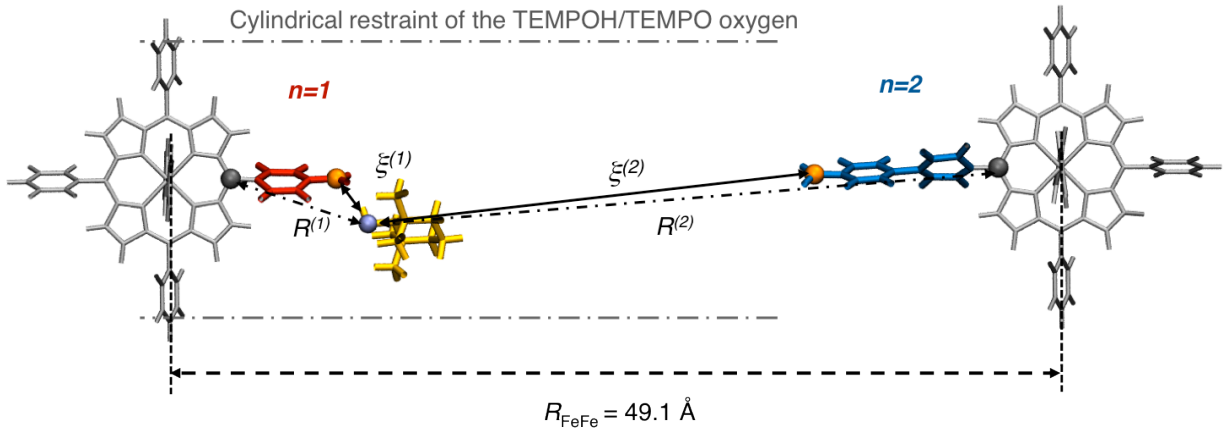

Figure S14. The system employed in molecular dynamics calculation of $\boldsymbol{w_{\mathrm{r}}^{(n)}(R)}$. Fixed regions of the porphyrin molecules are indicated in gray, the flexible linker region of $\mathbf{Fe^{III}PhCO_2^-}$ is indicated in red, and the flexible linker region of $\mathbf{Fe^{III}Ph_2CO_2^-}$ is indicated in blue. The rigid TEMPOH molecule is yellow, and the TEMPOH oxygen atom is indicated in purple. The porphyrin *5*-carbon atoms defining the $R^{(1)}$ and $R^{(2)}$ distances (see text) are indicated with gray spheres, and the carboxylic carbons defining the $\boldsymbol{\xi^{(1)}}$ and $\boldsymbol{\xi^{(2)}}$ distances are indicated with orange spheres. MeCN molecules are omitted for clarity. The region of the application of cylindrical restraint $\boldsymbol{V_{\mathrm{cyl}}(d)}$ is indicated with gray dashed-dot lines.

To compute the reactant free energy profiles, we begin by defining collective variables associated with the electron donor-acceptor distance for the n=1 and n=2 complexes in the simulation setup. Specifically, $R^{(1)}$ and $R^{(2)}$ denote the Euclidean distance between the TEMPOH oxygen and the 5-carbon of the porphyrin ring of $\mathbf{Fe^{III}PhCO_2^-}$ or $\mathbf{Fe^{III}Ph_2CO_2^-}$, respectively (Fig. S14). We then define $\Delta R = R^{(1)} - R^{(2)}$ and $R = \min(R^{(1)}, R^{(2)})$ in terms of these simple donor-acceptor distances. It is clear that any atomistic configuration for the system corresponds to a particular value for the collective variables ΔR and R. Furthermore, it is clear that the collective variables distinguish between configurations for which the system occupies the basin of stability for the n=1 complex (small R, negative ΔR), for which the system occupies the basin

of stability for the n=2 complex (small R, positive ΔR), and for which the system is transferring between these two basins of stability (larger R, $\Delta R \approx 0$).

By sampling the full probability distribution in these two coordinates, $P_{\mathrm{r}}(\Delta R, R)$, we have a direct means of comparing the relative free energies of these two basins of stability (i.e. the difference of the reversible work of association for the n=1 and n=2 TEMPOH-$\mathbf{Fe^{III}Ph}_n\mathbf{CO_2^-}$ complexes). Specifically, this relative free energy can be evaluated using

$$-kT \ln \int_{-\infty}^{c} d\Delta R \int_{0}^{\infty} dR\, P_{\mathrm{r}}(\Delta R, R) + kT \ln \int_{c}^{\infty} d\Delta R \int_{0}^{\infty} dR\, P_{\mathrm{r}}(\Delta R, R)\,, \qquad \text{(S18)}$$

where $c \approx 0$ is the value of ΔR that is used to distinguish between the two basins of stability. We can also reduce the probability distribution $P_{\mathrm{r}}(\Delta R, R)$ over the configurations associated with $\Delta R < c$ to obtain the reversible work associated with the electron donor-acceptor distance for the n=1 complex,

$$w_{\mathrm{r}}^{(1)}(R) = -kT \ln \int_{-\infty}^{c} d\Delta R\, P_{\mathrm{r}}(\Delta R, R)\,, \qquad \text{(S19)}$$

and we can likewise reduce the probability distribution over the configurations associated with $\Delta R > c$ to obtain the reversible work associated with the electron donor-acceptor distance for the n=2 complex,

$$w_{\mathrm{r}}^{(2)}(R) = -kT \ln \int_{c}^{\infty} d\Delta R\, P_{\mathrm{r}}(\Delta R, R)\,. \qquad \text{(S20)}$$

The advantage of this approach is that we have avoided any arbitrary shift between the curves $w_{\mathrm{r}}^{(1)}(R)$ and $w_{\mathrm{r}}^{(2)}(R)$, since both curves are obtained from the same full probability distribution $P_{\mathrm{r}}(\Delta R, R)$. That is, the relative energy of these two curves can be directly compared.

In practice, the MD sampling of $P_{\mathrm{r}}(\Delta R, R)$ involves slow timescales that are difficult to converge, and it is more convenient to sample the three-dimensional probability distribution $P_{\mathrm{r}}(\Delta\xi, \xi, R)$. Here, $R = \min(R^{(1)}, R^{(2)})$ as before, $\Delta\xi = \xi^{(1)} - \xi^{(2)}$, and $\xi = \min(\xi^{(1)}, \xi^{(2)})$. The collective variables $\xi^{(1)}$ and $\xi^{(2)}$ denote the distance between the TEMPOH oxygen and the carboxylic carbon of $\mathbf{Fe^{III}PhCO_2^-}$ or $\mathbf{Fe^{III}Ph_2CO_2^-}$, respectively (Fig. S14). We then reduce this three-dimensional distribution to recover the reversible work profiles,

$$w_{\mathrm{r}}^{(1)}(R) = -kT \ln \int_{-\infty}^{c} d\Delta\xi \int_{0}^{\infty} d\xi\, P_{\mathrm{r}}(\Delta\xi, \xi, R) = -kT \ln \int_{-\infty}^{c} d\Delta\xi\, P_{\mathrm{r}}(\Delta\xi, R) \qquad \text{(S21)}$$

and

$$w_{\mathrm{r}}^{(2)}(R) = -kT \ln \int_{c}^{\infty} d\Delta\xi \int_{0}^{\infty} d\xi\, P_{\mathrm{r}}(\Delta\xi, \xi, R) = -kT \ln \int_{c}^{\infty} d\Delta\xi\, P_{\mathrm{r}}(\Delta\xi, R)\,. \qquad \text{(S22)}$$

Computation of the three-dimensional probability distribution, $P_{\mathrm{r}}(\Delta\xi, \xi, R)$, is performed using umbrella sampling and the weighted histogram analysis method (WHAM).[28] Two-dimensional umbrella sampling is performed with respect to coordinates $\Delta\xi$ and ξ; this consists of 73 independent MD trajectories in the region $\Delta\xi = [-18\ \text{Å}, 18\ \text{Å}]$ that are harmonically restrained to uniformly spaced values of $\Delta\xi$, using a restraint force constant of 2.0 kcal/mol/Å^2. Furthermore, the regions of $\xi^{(1)} = [4\ \text{Å}, 7\ \text{Å}]$ and $\xi^{(2)} = [4\ \text{Å}, 7\ \text{Å}]$ are each sampled with 7 additional simulations restrained to values of ξ spaced every 0.5 Å, using a restraint force constant of 8.0 kcal/mol/Å^2. All umbrella-sampling simulations are equilibrated for 0.5 ns prior to a 5 ns production run. The $\Delta\xi$, ξ, and R coordinates of the system are then sampled every 500 fs.

---

(28) (a) Kumar, S.; Bouzida, D.; Swendsen, R. H.; Kollman, P. A.; Rosenberg, J. M. *J. Comput. Chem.* **1992,** *13*, 1011. (b) Kumar, S.; Rosenberg, J. M.; Bouzida, D.; Swendsen, R. H.; Kollman, P. A. *J. Comput. Chem.* **1995,** *16*, 1339.

To confine the TEMPOH molecule to the vicinity of the iron-porphyrin molecules in the umbrella sampling trajectories, the physical potential energy function is modified to include the cylindrically symmetric term

$$V_{\mathrm{cyl}}(d) = \begin{cases} 0.5\, k\, \left(d - r_{\mathrm{cyl}}\right)^2 & d \geq r_{\mathrm{cyl}} \\ 0 & d < r_{\mathrm{cyl}} \end{cases}, \tag{S23}$$

where $d = \sqrt{(x_{\mathrm{o}} - x_{\mathrm{c}})^2 + (z_{\mathrm{o}} - z_{\mathrm{c}})^2}$, x_{o} and z_{o} are respectively the *x*- and *z*-coordinates of the TEMPOH oxygen atom, x_{c} and z_{c} are respectively the *x*- and *z*-coordinates of the *5*-carbons of the porphyrin rings, k =1.0 kcal/mol Å^{-2}, and r_{cyl}= 8.0 Å. This term restricts the accessible configuration space of the TEMPOH molecule with respect to the fixed axis that separates the two iron-porphyrin molecules; all other molecules in the system, including the solvent molecules, are unaffected. The parameter r_{cyl} is chosen to be sufficiently large to avoid any biases in the distribution of configurations for which TEMPOH is hydrogen bonded to the iron-porphyrin molecules.

The product free-energy profiles, $w_{\mathrm{p}}^{(1)}(R)$ and $w_{\mathrm{p}}^{(2)}(R)$, are computed using the same approach that is described above for the reactant species. The MD simulations on the product species likewise include the restraining potential in eq S23, with distances defined in terms of the TEMPO (as opposed to the TEMPOH) oxygen atom. However, to be consistent with the fact that the reactant free-energy profile is obtained with TEMPOH held rigid in its more stable *anti* conformation of the OH torsion, an additional restraining potential is included in the calculation of the product free-energy profile to enforce the *anti* conformation of the TEMPO-**Fe$^{\mathrm{II}}$Ph$_n$CO$_2$H** hydrogen bond. This additional restraining potential is given by

$$V(\phi, r_{\mathrm{OH}}) = V_{\mathrm{dih}}(\phi) S(r_{\mathrm{OH}}), \tag{S24}$$

where $V_{\mathrm{dih}}(\phi)$ is a piecewise torsional potential

$$V_{\mathrm{dih}}(\phi) = \begin{cases} 0 & \phi_0 - \Delta\phi < \phi < \phi_0 + \Delta\phi \\ 0.5\, k_\phi\, (\phi - (\,\phi_0 + \Delta\phi))^2 & \phi > \phi_0 + \Delta\phi \\ 0.5\, k_\phi\, (\phi - (\,\phi_0 - \Delta\phi))^2 & \phi < \phi_0 - \Delta\phi \end{cases}, \tag{S25}$$

and $S(r_{\mathrm{OH}})$ is the sigmoid function

$$S(r_{\mathrm{OH}}) = 0.5(1 + \mathrm{erf}\,(2.0(-r_{\mathrm{OH}} + 3.0\ \text{Å})\,). \tag{S26}$$

Here, ϕ is the dihedral angle formed by the TC1, TN, and OC atoms of the TEMPO molecule and the HT atom of the nearest carboxylic acid, and r_{OH} is the distance between the OC atom and the HT atom. This restraint thus applies when TEMPO is hydrogen-bound to the carboxylic acid moiety of **Fe$^{\mathrm{II}}$PhCO$_2$H** or **Fe$^{\mathrm{II}}$Ph$_2$CO$_2$H**, and it does not bias the simulation when TEMPO is free in solution. We use parameters $\Delta\phi = 1.5$ rad, $\phi_0 = 1.5$ rad, and k_ϕ=3.0 kcal/mol/rad^2.

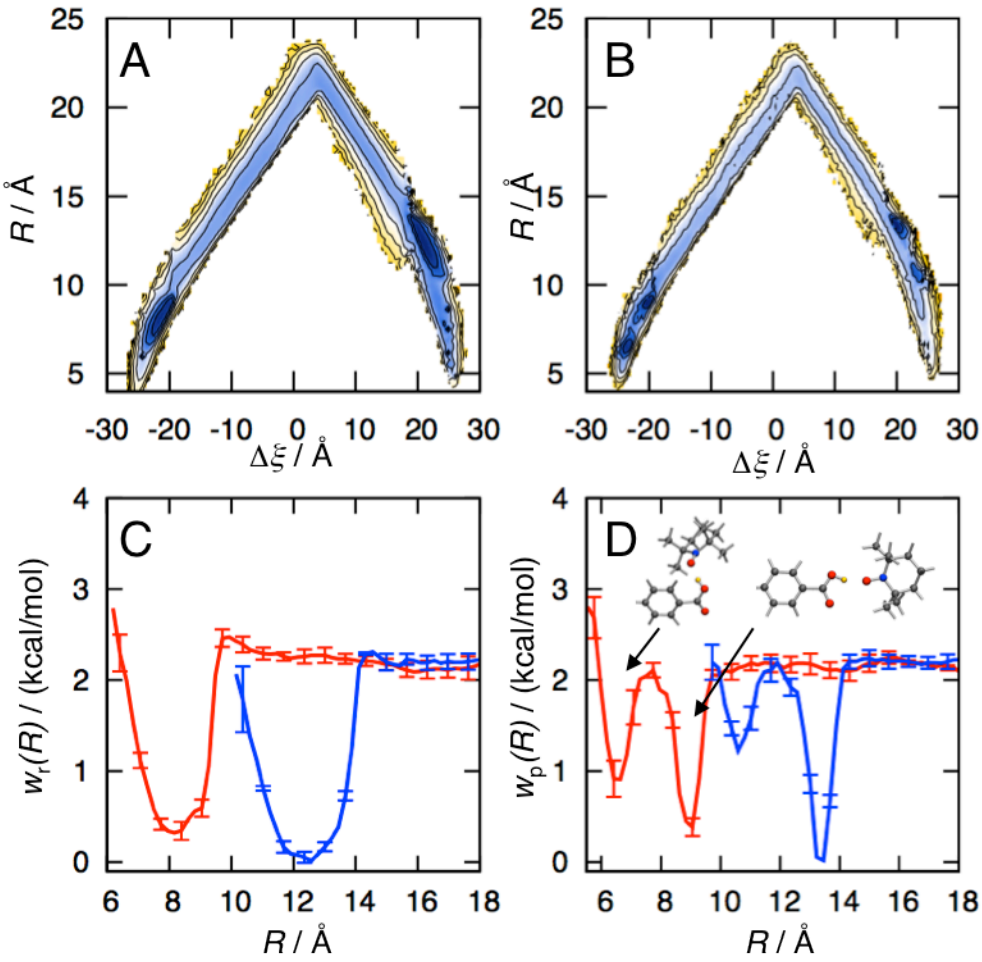

Figure S15. Free energy surfaces obtained using MD simulations. (A) The two-dimensional reactant free energy surface, $-\boldsymbol{kT}\ \mathbf{ln}\ \boldsymbol{P}_{\mathrm{r}}(\Delta\boldsymbol{\xi}, \boldsymbol{R})$. (B) The two-dimensional product free energy surface, $-\boldsymbol{kT}\ \mathbf{ln}\ \boldsymbol{P}_{\mathrm{p}}(\Delta\boldsymbol{\xi}, \boldsymbol{R})$. In panels A and B, the contour lines denote increments of 1 kcal/mol. (C) The reactant free energy profiles, $\boldsymbol{w}_{\mathrm{r}}^{(\boldsymbol{n})}(\boldsymbol{R})$, for the n=1 (red) and n=2 (blue) complexes as a function of the electron donor-acceptor distance. (D) The product free energy profiles, $\boldsymbol{w}_{\mathrm{p}}^{(\boldsymbol{n})}(\boldsymbol{R})$, for the n=1 (red) and n=2 (blue) complexes as a function of the electron donor-acceptor distance. The structures in panel D illustrate configurations of the TEMPO associated with different orientations of the carboxylic acid OH bond. The results in panels C and D are reproduced in Fig. 1 of the main text.

Figure S15A presents the free energy surface associated with the reduced two-dimensional probability distribution for the reactant species, $-kT\ \ln P_{\mathrm{r}}(\Delta\xi, R)$ (see eqs S21 and S22). The free energy surface is characterized by two pronounced basins of stability; the basin at $(\Delta\xi \approx -20\ \text{Å}, R \approx 8\ \text{Å})$ corresponds to the n=1 complex in which TEMPOH is bound to the $\mathbf{Fe^{III}PhCO_2^-}$ molecule, and the basin at $(\Delta\xi \approx +20\ \text{Å}, R \approx 12\ \text{Å})$ corresponds to the n=2 complex in which TEMPOH is bound to the $\mathbf{Fe^{III}Ph_2CO_2^-}$ molecule. The intermediate, featureless region for which $-20\ \text{Å} < \Delta\xi < 20\ \text{Å}$ corresponds to configurations for which the TEMPOH is not directly bound to either iron-porphyrin molecule. Figure S15B presents the free

energy surface associated with the reduced two-dimensional probability distribution for the product species, $-kT \ln P_{\mathrm{p}}(\Delta\xi, R)$, which also shows basins associated with the n=1 and n=2 complexes.

Figure S15C presents the one-dimensional free energy surfaces for the reactant species as a function of the electron donor-acceptor distance, $w_{\mathrm{r}}^{(1)}(R)$ and $w_{\mathrm{r}}^{(2)}(R)$, obtained by reducing the two-dimensional results in Figure S15A according to eqs S21 and S22. In these calculations, we use the parameter c=0 Å to separate the n=1 and n=2 basins of stability; the plotted results were found to be unchanged with the alternative choices of c=1 Å or 3 Å, indicating that the n=1 and n=2 basins of stability are well separated in the $\Delta\xi$ coordinate. Each curve in Figure S15C shows a single wide basin associated with the conformations of hydrogen-bound complex between TEMPOH the iron-porphyrin molecule. As expected from the presence of the additional phenylene linker, TEMPOH binds at larger values of R in the TEMPOH-$\mathbf{Fe^{III}Ph_2CO_2^-}$ complex than in the TEMPOH-$\mathbf{Fe^{III}PhCO_2^-}$ complex. Furthermore, TEMPOH-$\mathbf{Fe^{III}Ph_2CO_2^-}$ is more stable than TEMPOH-$\mathbf{Fe^{III}PhCO_2^-}$, with a free energy difference of 0.3 kcal/mol at the minimum of the basin. By considering the pairwise interaction energies between TEMPOH, the iron porphyrin molecule, and the acetonitrile solvent, we find that the hydrogen-bonded TEMPOH-$\mathbf{Fe^{III}Ph_2CO_2^-}$ complex is more favorably solvated than the TEMPOH-$\mathbf{Fe^{III}PhCO_2^-}$ complex relative to the separated TEMPOH and $\mathbf{Fe^{III}Ph_{\mathit{n}}CO_2^-}$molecules.

Figure S15D similarly presents the one-dimensional free energy surfaces for the product species as a function of the electron donor-acceptor distance, $w_{\mathrm{p}}^{(1)}(R)$ and $w_{\mathrm{p}}^{(2)}(R)$, obtained by reducing the two-dimensional results in Figure S15B. As is the case with the reactant species, the complex with the longer linker, TEMPO-$\mathbf{Fe^{II}Ph_2CO_2H}$, is more stable by ~0.3 kcal/mol and favors longer electron donor-acceptor distances than the TEMPO-$\mathbf{Fe^{II}PhCO_2H}$ complex. However, unlike the single, wide basin observed in the $w_{\mathrm{r}}^{(n)}(R)$ profiles, both $w_{\mathrm{p}}^{(1)}(R)$ and $w_{\mathrm{p}}^{(2)}(R)$ exhibit two narrow basins separated by ~ 3 Å. These additional features in the product free energy profiles are due to the torsional potential associated with rotation of the carboxylic acid OH bond, which exhibits local minima in configurations for which the acidic proton lies in the plane of the other of carboxylate atoms. As a result of this torsional potential, the acidic proton can either point away from the linker into solution, or it can point back towards the linker. The TEMPO molecule, which forms a hydrogen bond with the acidic proton, thus adopts two orientations that are characterized by differing values of the electron donor-acceptor distances. We illustrate these orientations in the inset of Figure S15D.

8.4. Calculation of CPET Reorganization Energies.

8.4.1. Inner-sphere Reorganization Energy.

The inner-sphere CPET reorganization energies, $\lambda_{\mathrm{i}}^{(n)}$, for reactions $1^{(n)}$ are computed as the sum of individual contributions from the iron-porphyrin complex and TEMPOH,[29]

$$\lambda_{\mathrm{i}}^{(n)} = \lambda_{\mathrm{i,FePor}}^{(n)} + \lambda_{\mathrm{i,TEMPOH}}. \qquad \text{(S27)}$$

The inner-sphere reorganization of the iron-porphyrin complex is calculated using[30]

$$\lambda_{\mathrm{i,FePor}}^{(n)} = \mathrm{E}(\mathrm{Fe^{II}Ph}_n\mathrm{CO_2H}|\mathrm{Fe^{III}Ph}_n\mathrm{CO_2^-}) - \mathrm{E}(\mathrm{Fe^{II}Ph}_n\mathrm{CO_2H}|\mathrm{Fe^{II}Ph}_n\mathrm{CO_2H}), \qquad \text{(S28)}$$

where $\mathrm{E(A|B)}$ denotes the energy of species A at the optimized geometry of species B. (In the calculation of $\mathrm{E}(\mathrm{Fe^{II}Ph}_n\mathrm{CO_2H}|\mathrm{Fe^{III}Ph}_n\mathrm{CO_2^-})$, the position of the additional proton is optimized while keeping all other atoms fixed.) The corresponding term for TEMPOH is calculated using

$$\lambda_{\mathrm{i,TEMPOH}} = \mathrm{E(TEMPO|TEMPOH)} - \mathrm{E(TEMPO|TEMPO)}. \qquad \text{(S29)}$$

By treating these contributions separately, we make the usual assumption that the inner-sphere reorganization energies are unaffected by preorganization of the CPET donor and acceptor species. In all cases, the geometry optimizations are performed at the B3LYP/6-31G(d,p) level of theory, with solvation effects included via the polarizable continuum model using the default parameters for Gaussian 09 (version G09RevB.01); final energies are computed using B3LYP/TZVP without implicit solvent effects.

These calculations yield $\lambda_{\mathrm{i,TEMPOH}} = 16.74$ kcal/mol, $\lambda_{\mathrm{i,FePor}}^{(1)} = 8.21$ kcal/mol, and $\lambda_{\mathrm{i,FePor}}^{(2)} = 8.37$ kcal/mol. The majority of the reorganization energy for the porphyrin molecules arises from the structural rearrangement of the acid moiety upon protonation, with the rearrangements in the porphyrin ring and its substituents contributing only ~ 1 kcal/mol; this is confirmed by repeating the calculation of $\mathrm{E}(\mathrm{Fe^{II}Ph}_n\mathrm{CO_2H}|\mathrm{Fe^{III}Ph}_n\mathrm{CO^{2-}})$ while fixing the position of atoms other than the carboxylic acid moiety. The small inner-sphere reorganization energy for the porphyrin obtained here is consistent with previous studies of model heme compounds, where the total inner-sphere reorganization energy in a self-exchange ET reaction between Fe^{III}(porphine)$(Im)_2$ and Fe^{II}(porphine)$(Im)_2^-$ was shown to be only 1.95 kcal/mol.[31] Similarly, the insensitivity of $\lambda_{\mathrm{i,FePor}}^{(n)}$to number of phenylene linkers is consistent with earlier computational studies of unmetalated *N*-methylmesoporphyrin, in which the structure of the porphyrin macrocycle was shown to be largely independent of the side chains decorating the ring.[32]

---

(29) (a) Hatcher, E.; Soudackov, A. V.; Hammes-Schiffer, S. *J. Am. Chem. Soc.* **2004**, *126,* 5763. (b) Iordanova, N.; Decornez, H.; Hammes-Schiffer, S. *J. Am. Chem. Soc.* **2001**, *123,* 3723.
(30) (a) Nelsen, S. F.; Blackstock, S. C.; Kim, Y. *J. Am. Chem. Soc.* **1987**, *109*, 677. (b) Markle, T. F.; Mayer, J. M. *Angew. Chem. Int. Ed.* **2008**, *47,* 738.
(31) Sigfridsson, E.; Olsson, M. H. M.; Ryde, U. *J. Phys. Chem. B* **1999**, *105*, 5546.
(32) Sigfridsson, E.; Ryde, U. *J. Biol. Inorg. Chem*. **2003**, *8*, 273.

8.4.2. Outer-sphere Reorganization Energy.

The outer-sphere CPET reorganization energy, $\lambda_{\mathrm{o}}^{(n)}(R)$, is calculated using the MD simulation model described in Sections 8.2 and 8.3. For reactions $1^{(n)}$, we obtain the outer-sphere reorganization energy for a given electron donor-acceptor distance R using[33]

$$\lambda_{\mathrm{o}}^{(n)}(R) = \tfrac{1}{2}\left(\langle \Delta U^{(n)} \rangle_{\mathrm{r}}(R) - \langle \Delta U^{(n)} \rangle_{\mathrm{p}}(R)\right), \tag{S30}$$

where

$$\langle \Delta U^{(n)} \rangle_{\mu}(R) = Z_R^{-1} \int d\mathbf{x}\, e^{-\frac{U_\mu(\mathbf{x})}{kT}} \delta(R(\mathbf{x}) - R) \Delta U^{(n)}(\mathbf{x}), \tag{S31}$$

$$Z_R = \int d\mathbf{x}\, e^{-\frac{U_\mu(\mathbf{x})}{kT}} \delta(R(\mathbf{x}) - R), \tag{S32}$$

and

$$\Delta U^{(n)}(\mathbf{x}) = U_{\mathrm{p}}^{(n)}(\mathbf{x}) - U_{\mathrm{r}}^{(n)}(\mathbf{x}). \tag{S33}$$

Here, $\mathbf{x}$ denotes the configuration of the solute and solvent, $U_\mu(\mathbf{x})$ is the total potential energy function for the system in the reactant ($\mu = \mathrm{r}$) or product ($\mu = \mathrm{p}$) state, and $U_\mu^{(n)}(\mathbf{x})$ denotes the subset of pairwise interactions between the acetonitrile solvent and the solute complex with *n* phenylene linkers. Equations S30-S32 are the *R*-resolved versions of the usual expressions for the outer-sphere reorganization energy, obtained by assuming that the linear response of the solvent holds for each value of the electron donor-acceptor distance, *R*. We additionally calculate the outer-sphere reorganization energy without resolving the dependence on *R* using

$$\lambda_{\mathrm{o}}^{(n)} = \frac{1}{2}\left(\langle \Delta U^{(n)} \rangle_{\mathrm{r}} - \langle \Delta U^{(n)} \rangle_{\mathrm{p}}\right) \tag{S34}$$

and

$$\langle \Delta U^{(n)} \rangle_{\mu} = Z^{-1} \int d\mathbf{x}\, e^{-\frac{U_\mu(\mathbf{x})}{kT}} \Delta U^{(n)}(\mathbf{x}). \tag{S35}$$

In the calculation of $\Delta U^{(n)}(\mathbf{x})$, the energy functions are evaluated at reactant and product geometries that are identical, except for the position of the transferring proton (HT). In the calculation of $\langle \Delta U^{(n)} \rangle_{\mathrm{r}}(R)$, the position of HT in the product state (needed for the $U_{\mathrm{p}}^{(n)}(\mathbf{x})$ term) is obtained via reflection of its position in the reactant state through the plane that perpendicularly bisects the segment between the TEMPOH oxygen (OC, the proton donor) and the acidic carboxylate oxygen (OA, the proton acceptor). For the calculation of $\langle \Delta U^{(n)} \rangle_{\mathrm{p}}(R)$, the reverse operation is performed to obtain the position of HT in the reactant state.

For the calculation of $\lambda_{\mathrm{o}}^{(1)}(R)$, the equilibrium ensemble for the reactant state is sampled using 1200 uncorrelated snapshots from an unrestrained, 6 ns NVT simulation of the system in the basin of stability for which TEMPOH is hydrogen-bonded to $\mathbf{Fe^{III}PhCO_2^-}$; the equilibrium ensemble for the product state is sampled using 1000 uncorrelated snapshots from an unrestrained, 5 ns NVT simulation of the system in the basin of stability for which TEMPO occupying is hydrogen-bonded to $\mathbf{Fe^{II}PhCO_2H}$. Similarly, for the calculation of $\lambda_{\mathrm{o}}^{(2)}(R)$, the equilibrium ensemble for the reactant state is sampled using 1500 uncorrelated snapshots from an unrestrained, 7.5 ns NVT simulation of the TEMPOH-$\mathbf{Fe^{III}Ph_2CO_2^-}$ complex; the equilibrium

(33) (a) Warshel, A. *J. Phys. Chem.* **1982**, *86*, 2218. (b) King, G.; Warshel, A. *J. Chem. Phys.* **1990**, *93*, 8682. (c) Small, D. W.; Matyushov, D. V.; Voth, G. A. *J. Am. Chem. Soc.* **2003**, *125*, 7470.

ensemble for the product state is sampled using 1000 uncorrelated snapshots from an unrestrained, 5 ns NVT simulation of the TEMPO-**Fe^{II}Ph$_2$CO$_2$H** complex.

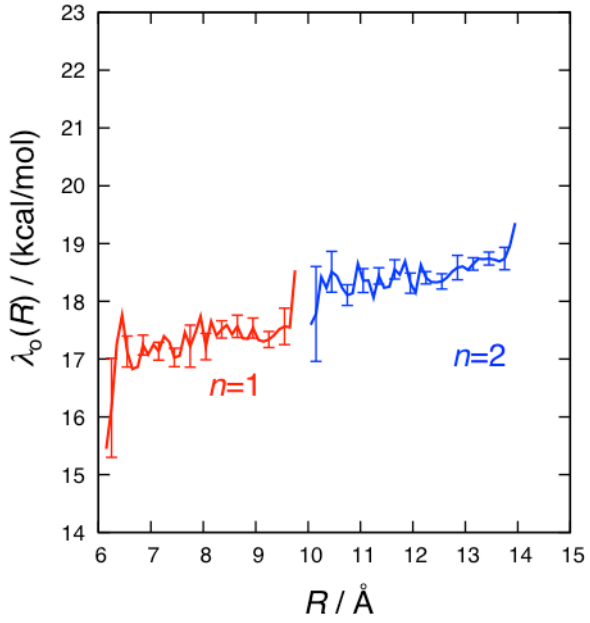

Figure S16. Outer-sphere CPET reorganization energies, $\boldsymbol{\lambda_o^{(n)}(R)}$, for the complexes with n=1 (red) and n=2 (blue) phenylene linkers, computing using all-atom MD simulations.

Figure S16 presents the computed CPET outer-sphere reorganization energies $\lambda_o^{(1)}(R)$ and $\lambda_o^{(2)}(R)$ as a function of the electron donor-acceptor distance. For a given number of phenylene linkers, the reorganization energy depends only weakly on R. It is also weakly sensitive to the number of linkers, n. If the R-dependence of the outer-sphere reorganization energy is not included (eqs. S34-S35), we obtain $\lambda_o^{(1)}$=17.6±0.1 kcal/mol and $\lambda_o^{(2)}$=18.9±0.1 kcal/mol.

8.4.3. Calculation of Outer-sphere Reorganization Energy using the Frequency-Resolved Cavity Model

For comparison, we also calculated the outer-sphere CPET reorganization energy using a dielectric continuum representation of the solvent. It is obtained using

$$\lambda_o^{(n)}(R) = Z_R^{-1} \int d\mathbf{x}\, e^{-\frac{U_r(\mathbf{x})}{kT}} \delta(R(\mathbf{x}) - R) \Delta S^{(n)}(\mathbf{x}), \tag{S36}$$

where

$$\Delta S^{(n)}(\mathbf{x}) = \frac{1}{2}\left[S_{pr}^{(n)}(\mathbf{x}) - S_{pp}^{(n)}(\mathbf{x}) + S_{rp}^{(n)}(\mathbf{x}) - S_{rr}^{(n)}(\mathbf{x})\right]. \tag{S37}$$

Here, $S_{AB}^{(n)}(\mathbf{x})$ denotes the interaction energy between the solute with the charge distribution for state A and the continuum solvent that is polarized in response to the charge distribution for state

B. $S_{\mathrm{AB}}^{(n)}(\mathbf{x})$ is computed using the frequency-resolved cavity model (FRCM),[34] for which the solute is represented as a set of overlapping atom-centered spherical cavities with sizes that correspond to the optical and static components of the solvent response. The reported calculations employ standard FRCM parameters for acetonitrile, including the global scaling factor for the atomic van der Waals radii used in computation of the solvent optical response (κ=0.9) and the solvent-specific additive factor for the atomic van der Waals radii used in computation of the solvent static response (δ=1.8 Å). The optical and static dielectric constants employed for the acetonitrile solvent are ε_o=37.5 and ε_∞ =1.79, respectively. The FRCM calculations are performed using the webPCET software package.[35]

For the calculation of $\lambda_{\mathrm{o}}^{(1)}(R)$, the solute configurations are obtained by taking 4000 uncorrelated configurations from an unrestrained, 8 ns simulation of the TEMPOH-$\mathbf{Fe^{III}PhCO_2^-}$ complex. Similarly, for $\lambda_{\mathrm{o}}^{(2)}(R)$ complex, the solute configurations are obtained by taking 3000 uncorrelated configurations from an unrestrained, 6 ns simulation of the TEMPOH-$\mathbf{Fe^{III}Ph_2CO_2^-}$ complex. For each configuration, the reactant and product geometries are identical, except for the position of the transferring proton (HT), which is obtained as in Section 8.4.2. The charge distributions for the reactant and product state of both complexes are described in Section 8.2.

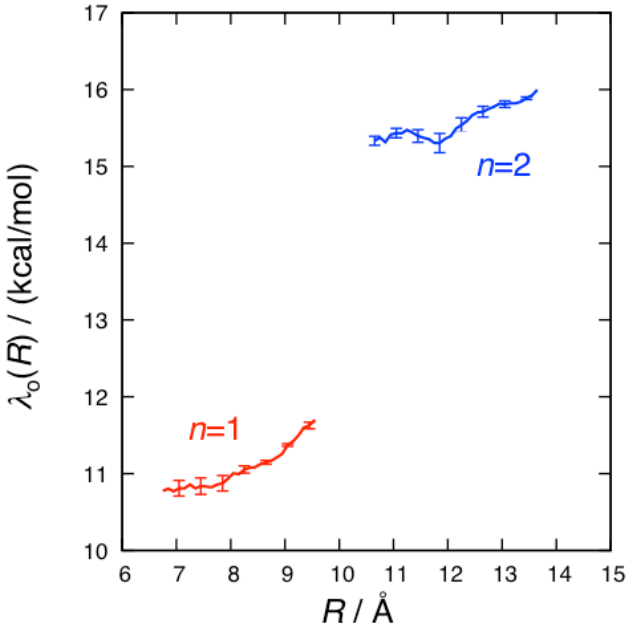

Figure S17. Outer-sphere CPET reorganization energies, $\boldsymbol{\lambda_{\mathrm{o}}^{(n)}(R)}$, for the complexes with n=1 (red) and n=2 (blue) phenylene linkers, computing using the FRCM.

(34) (a) Basilevsky, M. V.; Rostov, I. V.; Newton, M. D. *Chem. Phys.* **1998**, *232*, 189. (b) Newton, M. D.; Basilevsky, M. V.; Rostov, I. V. *Chem. Phys.* **1998**, *232*, 201.
(35) *web*PCET Application Server, Pennsylvania State University, http://webpcet.chem.psu.edu (2009).

Figure S17 presents the computed CPET outer-sphere reorganization energies $\lambda_o^{(1)}(R)$ and $\lambda_o^{(2)}(R)$ as a function of the electron donor-acceptor distance. For a given number of phenylene linkers, the reorganization energy depends relatively weakly on *R*. However, unlike the results obtained with explicit solvent (Fig. S16), the FRCM predicts a stronger difference in the outer-sphere reorganization energy upon changing the number of linkers, *n*. If the *R*-dependence of the outer-sphere reorganization energy is not included, we obtain $\lambda_o^{(1)}$=11.0±0.1 kcal/mol and $\lambda_o^{(2)}$=15.6±0.1 kcal/mol.

8.5. Calculation of $\Delta G^{o(n)}$ and $\Delta\Delta G^o$.

In this section, we validate the assumption that $\Delta G°$ is small in comparison to λ for the CPET reactions considered in this study, and we calculate the difference in the reaction driving forces at infinite separation, $\Delta\Delta G^o$, which appears in eq 6 in the main text.

For each complex, the driving force at infinite separation is calculated using

$$\Delta G_{\mathrm{CPET}}^{o(n)} = \mathrm{E}(\mathrm{Fe^{II}Ph}_n\mathrm{CO_2H}) + \mathrm{E(TEMPO)} - \mathrm{E}(\mathrm{Fe^{III}Ph}_n\mathrm{CO_2^-}) - \mathrm{E\ (TEMPOH)}\ , \quad \text{(S38)}$$

where E(A) represents the energy of species A. As before, geometry optimizations are performed at the B3LYP/6-31G(d,p) level of theory, with solvation effects included via the polarizable continuum model using the default parameters for Gaussian 09 (version G09RevB.01); final energies are computed using B3LYP/TZVP with implicit solvent effects included. We compute $\Delta G_{\mathrm{CPET}}^{o(1)} = -3.43$ kcal/mol, and $\Delta G_{\mathrm{CPET}}^{o(2)} = -3.69$ kcal/mol, which are in agreement with the experimental estimates of $\Delta G_{\mathrm{CPET}}^{o(1)} = -3.5 \pm 1.1$ kcal/mol and $\Delta G_{\mathrm{CPET}}^{o(2)} = -3.7 \pm 1.3$ kcal/mol. The values for $\Delta G°$ at finite separations, obtained using eq S12 and the results in Figs. S15C and S15D, are comparable or smaller in magnitude than the corresponding values for $\Delta G°$ at infinite separations.

The difference in the reaction driving forces at infinite separation is calculated as

$$\Delta\Delta G^o = \Delta G_{\mathrm{CPET}}^{o(1)} - \Delta G_{\mathrm{CPET}}^{o(2)}\ . \quad \text{(S39)}$$

Using the driving force values described above, we obtain $\Delta\Delta G^o$ = 0.26 kcal/mol, which is again in agreement with the experimentally measured value of $\Delta\Delta G^o = 0.2 \pm 1.4$ kcal/mol.

8.6. Decorrelation of the proton and electron donor-acceptor distances, and insensitivity of the proton donor-acceptor distance distribution to phenylene linker length.

Various simplifications in the derivation of the CPET rate expression (Section 8.1) follow from the assumption that the proton donor-acceptor distance, r, and the electron donor-acceptor distance, R, are statistically uncorrelated in the hydrogen-bonded configurations for the TEMPOH/iron-porphyrin system that dominantly contribute to the CPET rate. Furthermore, cancellation of γ in eq 6 in the main text is based on the assumption that the distribution of proton donor-acceptor distances is insensitive to the number of phenylene linkers in the iron-porphyrin complex. Here, we validate these assumptions using MD simulations. Employing the simulation setup for the reactant species that is described in Section 8.2, two unrestrained MD trajectories of length 5 ns are performed; for the first of these trajectories, the TEMPOH molecule occupies the basin of stability for which it is hydrogen-bonded to $\mathbf{Fe^{III}PhCO_2^-}$, and for

the second trajectory, the TEMPOH molecule occupies the basin of stability for which it is hydrogen-bonded to $\mathbf{Fe^{III}Ph_2CO_2^-}$. Configurations are sampled every 500 fs to construct the one-dimensional probability distributions $P_r(r)$ and $P_r(R)$, as well as the two-dimensional probability distribution $P_r(r, R)$.

Figure S18A presents the computed distribution of proton donor-acceptor distances, $P_r(r)$, for the TEMPOH-$\mathbf{Fe^{III}PhCO_2^-}$ and TEMPOH-$\mathbf{Fe^{III}Ph_2CO_2^-}$ systems. It is clear that the distributions are essentially identical for the two cases, both of which are peaked about 2.65 Å. These data are replotted in Fig. S18B in terms of the proton donor-acceptor free-energy profiles $w_r(r) = -kT \ln P_r(r)$. The results in Fig. S18B further emphasize that the work for compression of the proton donor-acceptor distances during the CPET reaction is insensitive to the number of phenylene linkers. These numerical results validate the cancellation of γ in the numerator and denominator of eq 6 in the main text, since the distribution of proton donor-acceptor distances is insensitive to the number of phenylene linkers.

Figure S18C addresses the issue of statistical decorrelation between the proton and electron donor-acceptor distances in the TEMPOH-$\mathbf{Fe^{III}PhCO_2^-}$ system. Plotted are cross-sections of the two-dimensional free-energy profile in the coordinates r and R, which is obtained using $w_r(r, R) = -kT \ln P_r(r, R)$. At various distances for the electron donor-acceptor distances (R = 7.5, 8, and 9 Å), the figure demonstrates that the proton donor-acceptor distribution is essentially unchanged, indicating that the proton and electron donor-acceptor distance distributions are uncorrelated. Figure S18D demonstrates that the same lack of correlation is found in the system with n=2 phenylene linkers. These numerical results validate the assumption that the proton and electron donor-acceptor distances are statistically uncorrelated in the hydrogen-bonded configurations of the TEMPOH/iron-porphyrin system.

The results in this section indicate that although the distribution of electron donor-acceptor distances is sensitive to the number of phenylene linkers (Figs. S15C and S15D), the proton donor-acceptor distance distribution is both insensitive to the number of phenylene linkers (Figs. S18A and S18B) and uncorrelated with the electron donor-acceptor distance distribution (Figs. S18C and S18D). The results validate key aspects of the experimental design, which aims to alter the electron donor-acceptor chemistry of the TEMPOH/iron-porphyrin systems through inclusion of phenylene linkers while leaving the proton-transfer interface between the TEMPOH and iron-porphyrin complexes unchanged.

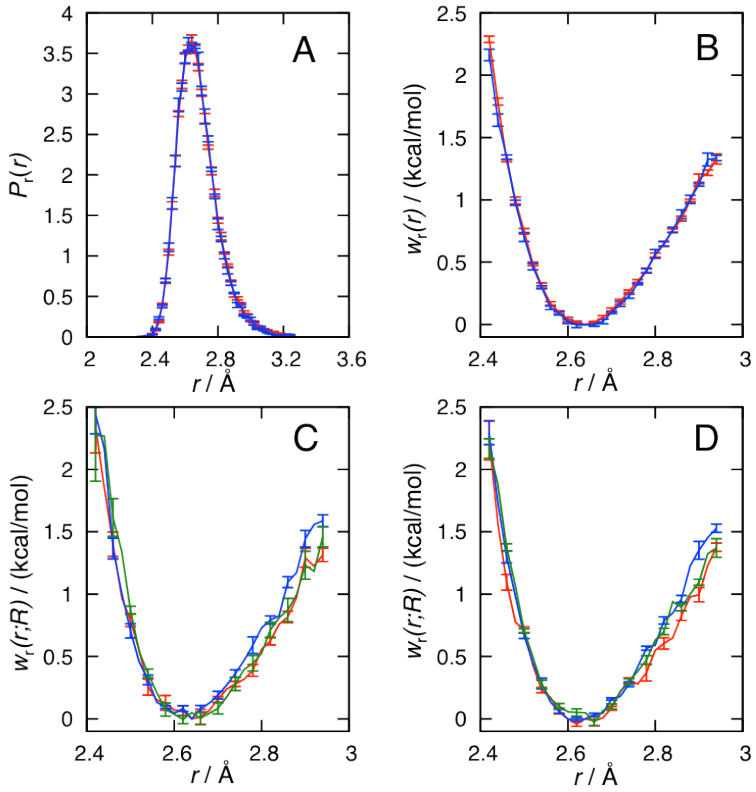

Figure S18. (A) Distribution of r, the proton donor-acceptor distances in the n=1 (red) and n=2 (blue) TEMPOH/iron-porphyrin complexes. (B) $\boldsymbol{w}_{\mathrm{r}}^{(\boldsymbol{n})}(\boldsymbol{r})$, the free energy as a function of the proton donor-acceptor distance for the n=1 and n=2 complexes. (C) $\boldsymbol{w}_{\mathrm{r}}^{(\boldsymbol{1})}(\boldsymbol{r};\boldsymbol{R})$ at R=7.5 Å (blue) R=8 Å (red), and R=9 Å (green). (D) $\boldsymbol{w}_{\mathrm{r}}^{(\boldsymbol{2})}(\boldsymbol{r};\boldsymbol{R})$ at R=11.5 Å (blue) R=12 Å (red), and R=13 Å (green).

8.7. Molecular Geometries.

Table S4. Optimized Cartesian coordinates of the TEMPO molecule

Center Number	Atomic Number	X / Å	Y / Å	Z / Å
1	1	3.320078	-0.33139	-0.839409
2	1	2.796467	0.162893	1.56301
3	1	2.160467	1.908445	-0.164171
4	6	2.345462	-0.824398	-0.904682
5	1	2.452383	-1.859515	-0.577743
6	1	2.028075	-0.821484	-1.951866
7	6	1.24656	1.39869	-0.488705
8	6	1.761902	-0.176348	1.451656
9	1	1.245477	1.423354	-1.586061
10	6	1.333331	-0.070526	-0.027102
11	1	1.699822	-1.216967	1.779945
12	1	1.136618	0.431737	2.109752
13	1	0.000003	3.158855	-0.353264
14	6	0.000002	2.127117	0.014728
15	1	0.000002	2.191361	1.109223
16	7	0	-0.746531	-0.19978
17	8	0	-2.026301	-0.060841
18	6	-1.246555	1.398688	-0.488708
19	1	-1.245465	1.423347	-1.586064
20	1	-1.136637	0.431749	2.109754
21	6	-1.333331	-0.070524	-0.027102
22	6	-1.761906	-0.176346	1.451653
23	1	-2.160463	1.908448	-0.164183
24	1	-1.699817	-1.216964	1.779944
25	6	-2.345462	-0.824393	-0.904681
26	1	-2.028068	-0.821496	-1.951864
27	1	-2.796478	0.16288	1.563
28	1	-2.4524	-1.859507	-0.577735
29	1	-3.320074	-0.331375	-0.839421

Table S5. Optimized Cartesian coordinates of the TEMPOH molecule

Center Number	Atomic Number	X / Å	Y / Å	Z / Å
1	1	-1.479624	-1.209808	1.801593
2	6	-1.634694	-0.180922	1.469249
3	6	-1.295588	-0.049098	-0.0331
4	6	-1.2513	1.433314	-0.468764
5	1	-1.279652	1.473653	-1.565388
6	1	-2.162053	1.925904	-0.10904
7	6	0.000014	2.16908	0.016436
8	1	0.000039	3.196869	-0.364593
9	6	1.251225	1.433274	-0.468908
10	1	1.279219	1.473324	-1.565547
11	1	2.162039	1.92601	-0.10957
12	6	1.295622	-0.049118	-0.033077
13	6	2.395467	-0.766722	-0.839401
14	1	2.160771	-0.745813	-1.908204
15	1	3.360783	-0.273358	-0.686656
16	1	2.492708	-1.809506	-0.527038
17	6	1.634669	-0.180846	1.469253
18	1	1.037224	0.478138	2.101323
19	1	2.68697	0.075343	1.631307
20	1	1.48086	-1.210026	1.801349
21	1	0.000053	2.248951	1.109867
22	6	-2.395369	-0.766738	-0.839511
23	1	-2.160288	-0.746249	-1.908234
24	1	-3.360615	-0.273092	-0.687241
25	1	-2.493027	-1.809391	-0.526763
26	7	0.000038	-0.66514	-0.446046
27	8	-0.000006	-2.041552	0.011015
28	1	-0.000332	-2.538979	-0.818379
29	1	-1.038231	0.479081	2.101259
30	1	-2.687339	0.074	1.631093

Table S6. Optimized Cartesian coordinates of the $\mathbf{Fe^{III}PhCO_2^-}$ molecule

Center Number	Atomic Number	X / Å	Y / Å	Z / Å
1	6	2.063901	3.447332	0.079828
2	1	2.206164	4.515452	0.135018
3	6	0.783962	2.789153	0.014438
4	6	-0.441389	3.467466	0.021413
5	6	-0.428342	4.965423	0.043228
6	6	0.01639	5.692989	-1.071868
7	6	0.029354	7.088415	-1.051338
8	1	0.372679	7.635569	-1.924207
9	6	-0.400711	7.777865	0.084403
10	1	-0.38987	8.86349	0.100307
11	6	-0.844516	7.0642	1.199714
12	1	-1.176826	7.592208	2.088505
13	1	0.347735	5.161135	-1.958727
14	6	-0.85886	5.668801	1.179286
15	1	-1.20052	5.117823	2.050448
16	6	-1.676654	2.808877	0.011743
17	6	-2.947243	3.488748	-0.004174
18	1	-3.073581	4.560227	-0.011125
19	6	-3.910129	2.532308	-0.005071
20	1	-4.980635	2.666791	-0.007257
21	6	-3.240278	1.256052	-0.00873
22	6	-3.912803	0.029712	-0.014434
23	6	-5.411658	0.040246	-0.034442
24	6	-6.109262	0.43451	-1.186746
25	1	-5.553634	0.730119	-2.071715
26	6	-7.50491	0.442479	-1.204728
27	1	-8.029308	0.746622	-2.105692
28	6	-8.223611	0.057227	-0.070967
29	1	-9.309323	0.063844	-0.085034
30	6	-7.5393	-0.336707	1.080912
31	1	-8.090567	-0.634577	1.967833
32	6	-6.143663	-0.345799	1.09913
33	1	-5.614813	-0.648563	1.997968
34	6	-3.259799	-1.207086	-0.004966
35	7	-1.896178	-1.415417	0.026256
36	26	-0.467811	0.002403	0.002069
37	7	-0.491767	-0.006921	-2.002898
38	6	-0.428887	1.091288	-2.843615

39	1	-0.35927	2.096582	-2.464383
40	6	-0.469906	0.667266	-4.142533
41	1	-0.444436	1.204039	-5.076534
42	7	-0.558695	-0.706004	-4.082991
43	1	-0.607693	-1.337775	-4.869959
44	6	-0.569634	-1.076787	-2.786858
45	1	-0.633759	-2.101537	-2.461566
46	7	-0.442117	0.011725	2.007483
47	6	-0.360294	1.081314	2.79148
48	1	-0.29649	2.106101	2.466323
49	7	-0.365199	0.710212	4.087541
50	1	-0.309781	1.341603	4.874386
51	6	-0.453658	-0.663049	4.147133
52	1	-0.47367	-1.200178	5.081062
53	6	-0.501032	-1.086659	2.848314
54	1	-0.57162	-2.091943	2.469354
55	7	0.936895	-1.437453	-0.00212
56	6	2.304347	-1.251115	-0.005187
57	6	2.9792	-0.025106	0.000093
58	6	2.323502	1.211354	0.004824
59	6	4.47672	-0.034441	0.004588
60	6	5.199799	0.405979	-1.116274
61	1	4.661393	0.749017	-1.995728
62	6	6.593969	0.397027	-1.109168
63	1	7.158008	0.731751	-1.973561
64	6	7.308206	-0.046066	0.010357
65	6	8.847374	-0.051436	0.013785
66	6	6.585727	-0.48335	1.126945
67	1	7.143393	-0.822174	1.993883
68	6	5.191482	-0.480466	1.12858
69	1	4.646852	-0.817708	2.006429
70	6	2.973078	-2.527722	-0.020835
71	1	4.043421	-2.66148	-0.034018
72	6	2.010003	-3.483887	-0.007877
73	1	2.136109	-4.555395	-0.003701
74	6	0.739784	-2.803609	-0.007197
75	6	-0.49586	-3.4627	-0.00556
76	6	-0.509047	-4.960917	-0.020054
77	6	-0.092858	-5.66979	-1.158
78	1	0.238686	-5.123108	-2.035756
79	6	-0.107817	-7.065257	-1.171563

80	1	0.213828	-7.597607	-2.061681
81	6	-0.538218	-7.773466	-0.047532
82	6	-0.954215	-7.078477	1.090037
83	1	-1.286854	-7.621354	1.9697
84	1	-0.549254	-8.859155	-0.058038
85	6	-0.940444	-5.682924	1.103775
86	1	-1.260624	-5.146754	1.992152
87	6	-1.720851	-2.785037	0.002328
88	6	-3.001232	-3.443662	-0.054601
89	1	-3.143569	-4.51235	-0.097495
90	6	-3.948722	-2.471788	-0.058809
91	1	-5.020364	-2.588486	-0.104964
92	7	-1.87341	1.4425	0.005094
93	7	0.95942	1.419987	-0.022491
94	6	3.011568	2.475596	0.073448
95	1	4.083117	2.590825	0.121601
96	8	9.406957	0.359911	-1.038303
97	8	9.399312	-0.466396	1.06847

Table S7. Optimized Cartesian coordinates of the **$Fe^{II}PhCO_2H$** molecule

Center Number	Atomic Number	X / Å	Y / Å	Z / Å
1	6	2.050838	3.457774	0.072409
2	1	2.194236	4.526615	0.123998
3	6	0.769848	2.788161	0.009671
4	6	-0.462272	3.460009	0.016105
5	6	-0.449627	4.959147	0.033336
6	6	-0.005848	5.68693	-1.082684
7	6	0.008459	7.082745	-1.068378
8	1	0.3522	7.626301	-1.943721
9	6	-0.421403	7.777802	0.064143
10	1	-0.410539	8.863658	0.076027
11	6	-0.86513	7.066918	1.181423
12	1	-1.197692	7.597973	2.068678
13	1	0.326429	5.15152	-1.967229
14	6	-0.87866	5.67113	1.165245
15	1	-1.221166	5.123653	2.038454
16	6	-1.704905	2.806247	0.009963
17	6	-2.976845	3.495968	-0.001301
18	1	-3.105198	4.567931	-0.005184
19	6	-3.940764	2.540297	-0.00273
20	1	-5.011473	2.678755	-0.002125
21	6	-3.263428	1.261564	-0.01032
22	6	-3.93108	0.028177	-0.013687
23	6	-5.430704	0.037993	-0.027238
24	6	-6.138465	0.449542	-1.168005
25	1	-5.587377	0.760458	-2.050726
26	6	-7.534443	0.457999	-1.180213
27	1	-8.062944	0.776666	-2.074096
28	6	-8.248937	0.0542	-0.050109
29	1	-9.334884	0.060595	-0.058882
30	6	-7.557611	-0.358103	1.091249
31	1	-8.104184	-0.670912	1.9763
32	6	-6.161633	-0.365975	1.101558
33	1	-5.628459	-0.683935	1.992738
34	6	-3.281957	-1.215074	-0.007282
35	7	-1.919195	-1.41596	0.020104
36	26	-0.488308	0.001882	0.000056

37	7	-0.507308	-0.011646	-2.0247
38	6	-0.49658	1.083944	-2.869813
39	1	-0.477522	2.090219	-2.485101
40	6	-0.514446	0.662868	-4.1724
41	1	-0.513766	1.200001	-5.106986
42	7	-0.536384	-0.713728	-4.114545
43	1	-0.55391	-1.34631	-4.901153
44	6	-0.531282	-1.079643	-2.810387
45	1	-0.546261	-2.10534	-2.480556
46	7	-0.468204	0.01543	2.024736
47	6	-0.444908	1.083459	2.810402
48	1	-0.431269	2.109174	2.48056
49	7	-0.438764	0.717552	4.114554
50	1	-0.421547	1.350151	4.901155
51	6	-0.459378	-0.659063	4.172429
52	1	-0.459135	-1.196188	5.10702
53	6	-0.477494	-1.080167	2.869856
54	1	-0.495894	-2.086461	2.485159
55	7	0.921203	-1.438157	0.000987
56	6	2.286553	-1.259447	0.013048
57	6	2.952422	-0.024434	0.014045
58	6	2.305144	1.220426	0.005153
59	6	4.449677	-0.034253	0.027515
60	6	5.181462	0.414615	-1.085171
61	1	4.649366	0.765521	-1.963605
62	6	6.573526	0.40839	-1.079405
63	1	7.121706	0.753198	-1.948516
64	6	7.269149	-0.04993	0.048653
65	6	8.752509	-0.077801	0.108916
66	6	6.54931	-0.499099	1.164529
67	1	7.093898	-0.846939	2.035544
68	6	5.158813	-0.490815	1.1525
69	1	4.609692	-0.834624	2.023222
70	6	2.963493	-2.538901	0.001638
71	1	4.033721	-2.681218	-0.002169
72	6	1.998917	-3.493739	-0.002107
73	1	2.127087	-4.565702	-0.001338
74	6	0.727434	-2.803526	-0.011433
75	6	-0.514916	-3.456233	-0.016504
76	6	-0.528551	-4.955393	-0.034143
77	6	-0.103128	-5.667341	-1.167404

78	1	0.23724	-5.119858	-2.041453
79	6	-0.117437	-7.063145	-1.183844
80	1	0.21244	-7.59419	-2.072106
81	6	-0.558475	-7.774002	-0.06551
82	6	-0.984853	-7.078935	1.068346
83	1	-1.326484	-7.622497	1.944511
84	1	-0.569967	-8.859849	-0.077575
85	6	-0.969719	-5.683149	1.082929
86	1	-1.299347	-5.147748	1.96847
87	6	-1.747297	-2.783372	-0.008745
88	6	-3.028773	-3.452628	-0.069466
89	1	-3.172374	-4.521598	-0.118275
90	6	-3.977963	-2.482288	-0.067601
91	1	-5.049836	-2.603164	-0.114432
92	7	-1.89737	1.44133	-0.000095
93	7	0.943045	1.420295	-0.020898
94	6	3.000715	2.488263	0.068978
95	1	4.072059	2.612752	0.119306
96	8	9.340004	0.376474	-1.020588
97	8	9.401384	-0.465301	1.066228
98	1	10.300786	0.318569	-0.882452

Table S8. Optimized Cartesian coordinates for the $Fe^{III}Ph_2CO_2^-$ molecule

Center Number	Atomic Number	X / Å	Y / Å	Z / Å
1	6	0.987469	3.457369	0.218613
2	1	1.122587	4.52391	0.31016
3	6	-0.287506	2.793712	0.114915
4	6	-1.51593	3.465496	0.087489
5	6	-1.515046	4.96301	0.125732
6	6	-1.017549	5.704674	-0.957655
7	6	-1.018281	7.099814	-0.924947
8	1	-0.633719	7.65745	-1.773633
9	6	-1.51494	7.775542	0.191701
10	1	-1.514637	8.861024	0.217345
11	6	-2.012196	7.048253	1.275099
12	1	-2.397012	7.565434	2.148924
13	1	-0.63543	5.183635	-1.830332
14	6	-2.013485	5.652997	1.242199
15	1	-2.39802	5.093149	2.089377
16	6	-2.74506	2.799326	0.007603
17	6	-4.017001	3.470017	-0.088097
18	1	-4.150023	4.540617	-0.104507
19	6	-4.971169	2.506585	-0.150664
20	1	-6.040413	2.63293	-0.221172
21	6	-4.29399	1.235371	-0.104402
22	6	-4.957879	0.004695	-0.122204
23	6	-6.45354	0.006777	-0.228989
24	6	-7.079832	0.329327	-1.442646
25	1	-6.47164	0.57553	-2.307994
26	6	-8.471906	0.329875	-1.545406
27	1	-8.94117	0.578507	-2.49261
28	6	-9.257383	0.008509	-0.436348
29	1	-10.340252	0.009088	-0.516361
30	6	-8.643885	-0.313202	0.776208
31	1	-9.24766	-0.56096	1.644137
32	6	-7.25176	-0.314338	0.879568
33	1	-6.778093	-0.561062	1.825093
34	6	-4.300666	-1.226987	-0.042981
35	7	-2.937628	-1.425272	0.038334
36	26	-1.519216	0.000174	0.032269
37	7	-1.5049	-0.01335	-1.970836

38	6	-1.372224	1.078095	-2.811964
39	1	-1.259841	2.079552	-2.43254
40	6	-1.409341	0.65252	-4.110547
41	1	-1.340155	1.18451	-5.045073
42	7	-1.566215	-0.71464	-4.049891
43	1	-1.631391	-1.345324	-4.836571
44	6	-1.620396	-1.080781	-2.753475
45	1	-1.739948	-2.100174	-2.426536
46	7	-1.535522	0.010646	2.039817
47	6	-1.71387	1.069455	2.822555
48	1	-1.876674	2.082256	2.495529
49	7	-1.662132	0.704795	4.119418
50	1	-1.768889	1.330658	4.905365
51	6	-1.441481	-0.653197	4.181377
52	1	-1.361532	-1.183109	5.116218
53	6	-1.364194	-1.074312	2.883282
54	1	-1.197229	-2.069081	2.507245
55	7	-0.105392	-1.4304	0.044587
56	6	1.260159	-1.235443	0.015077
57	6	1.92458	-0.004299	0.028374
58	6	1.261883	1.227374	0.068154
59	6	3.42178	-0.001723	0.012173
60	6	4.126096	0.442424	-1.117215
61	1	3.576688	0.79057	-1.986865
62	6	5.518808	0.444193	-1.136726
63	6	6.263809	0.004821	-0.028109
64	6	5.552392	-0.435474	1.102057
65	1	6.095225	-0.798295	1.969277
66	6	4.15967	-0.43955	1.122422
67	1	3.63706	-0.788219	2.008185
68	6	1.937121	-2.507615	-0.008616
69	1	3.00776	-2.63625	-0.042874
70	6	0.980871	-3.469946	0.033573
71	1	1.114451	-4.54049	0.044116
72	6	-0.293775	-2.798182	0.053715
73	6	-1.525356	-3.463367	0.08655
74	6	-1.531629	-4.961391	0.1199
75	6	-1.13503	-5.706479	-1.001601
76	1	-0.823521	-5.188576	-1.903831
77	6	-1.144187	-7.101688	-0.96725
78	1	-0.837599	-7.662968	-1.844824

79	6	-1.549986	-7.772749	0.188307
80	6	-1.947507	-7.041124	1.309396
81	1	-2.261747	-7.555029	2.21289
82	1	-1.55674	-8.858196	0.214714
83	6	-1.939112	-5.645824	1.275526
84	1	-2.245346	-5.080211	2.150498
85	6	-2.754264	-2.792806	0.074177
86	6	-4.029643	-3.461645	0.016544
87	1	-4.164746	-4.532157	0.016971
88	6	-4.981531	-2.497146	-0.060439
89	1	-6.050894	-2.622317	-0.13118
90	7	-2.931785	1.43143	-0.006371
91	7	-0.102525	1.427576	0.038867
92	6	1.941841	2.492839	0.183917
93	1	3.01226	2.614195	0.244248
94	6	7.748307	0.004008	-0.050592
95	6	8.455835	-0.30382	-1.227218
96	6	9.848827	-0.307725	-1.243499
97	1	10.394793	-0.554961	-2.148114
98	6	10.587758	-0.004763	-0.093323
99	6	12.125371	-0.013695	-0.115632
100	8	12.699968	0.26456	0.972023
101	8	12.664924	-0.299443	-1.219169
102	6	9.885633	0.304405	1.078096
103	1	10.459852	0.548309	1.965984
104	6	8.492738	0.30896	1.103809
105	1	7.973442	0.575738	2.020284
106	1	7.907571	-0.567592	-2.127539
107	1	6.035298	0.809936	-2.018704

Table S9. Optimized Cartesian coordinates for the $\mathbf{Fe^{II}Ph_2CO_2H}$ molecule

Center Number	Atomic Number	X / Å	Y / Å	Z / Å
1	6	0.970265	3.473582	0.054322
2	1	1.10683	4.543674	0.098814
3	6	-0.306668	2.795462	-0.002555
4	6	-1.543464	3.459452	-0.000066
5	6	-1.540952	4.958691	0.008694
6	6	-1.099656	5.6833	-1.11043
7	6	-1.095417	7.079232	-1.10433
8	1	-0.753436	7.620104	-1.982034
9	6	-1.533195	7.777841	0.022977
10	1	-1.530241	8.863805	0.028486
11	6	-1.974651	7.070279	1.143254
12	1	-2.313405	7.604097	2.026513
13	1	-0.761455	5.145123	-1.99104
14	6	-1.977961	5.674348	1.135259
15	1	-2.31885	5.129586	2.010803
16	6	-2.781623	2.797513	-0.004762
17	6	-4.058274	3.478331	-0.024152
18	1	-4.194017	4.549372	-0.033488
19	6	-5.015666	2.516046	-0.025744
20	1	-6.087302	2.647239	-0.0305
21	6	-4.329682	1.241905	-0.024139
22	6	-4.989023	0.003943	-0.02428
23	6	-6.488563	0.003681	-0.048828
24	6	-7.190189	0.403412	-1.197603
25	1	-6.634199	0.712794	-2.077796
26	6	-8.586052	0.402053	-1.221069
27	1	-9.109556	0.711622	-2.121082
28	6	-9.306787	0.000017	-0.094302
29	1	-10.392653	-0.001317	-0.111778
30	6	-8.621729	-0.400479	1.055011
31	1	-9.173196	-0.711776	1.937569
32	6	-7.225836	-0.398405	1.076533
33	1	-6.697686	-0.707275	1.973882
34	6	-4.33159	-1.234873	-0.005356
35	7	-2.967666	-1.426306	0.03092
36	26	-1.546283	0.001078	0.003874
37	7	-1.562342	-0.026074	-2.020594

38	6	-1.563837	1.063645	-2.87329
39	1	-1.557861	2.072705	-2.495431
40	6	-1.574366	0.633284	-4.172932
41	1	-1.578798	1.163816	-5.11128
42	7	-1.579292	-0.743064	-4.105497
43	1	-1.587532	-1.381279	-4.887684
44	6	-1.571775	-1.099753	-2.798732
45	1	-1.574448	-2.123177	-2.461507
46	7	-1.529644	0.028093	2.028679
47	6	-1.520533	1.10165	2.80702
48	1	-1.518429	2.125129	2.47003
49	7	-1.512534	0.744787	4.113728
50	1	-1.504593	1.382914	4.89599
51	6	-1.516862	-0.631556	4.180974
52	1	-1.512078	-1.16223	5.11924
53	6	-1.527476	-1.061735	2.881281
54	1	-1.533117	-2.070769	2.503413
55	7	-0.127217	-1.429254	0.016161
56	6	1.237272	-1.240501	0.02273
57	6	1.895866	-0.001895	0.01408
58	6	1.238838	1.237501	0.001089
59	6	3.394111	-0.001091	0.01928
60	6	4.1198	0.414283	-1.108411
61	1	3.584101	0.743386	-1.993674
62	6	5.51253	0.413744	-1.109095
63	6	6.237188	0.001121	0.022337
64	6	5.510672	-0.411248	1.152691
65	1	6.038873	-0.754634	2.036837
66	6	4.117793	-0.413754	1.149202
67	1	3.580903	-0.742634	2.033816
68	6	1.923062	-2.51489	0.024145
69	1	2.994528	-2.647706	0.021236
70	6	0.96538	-3.476827	0.033269
71	1	1.10112	-4.547819	0.045853
72	6	-0.311147	-2.795844	0.018076
73	6	-1.549295	-3.457234	0.018162
74	6	-1.55274	-4.956525	0.017269
75	6	-1.118092	-5.678744	-1.105998
76	1	-0.778166	-5.139082	-1.98507
77	6	-1.122587	-7.074703	-1.106239
78	1	-0.78559	-7.613707	-1.987018

79	6	-1.563029	-7.775666	0.018575
80	6	-1.99869	-7.070459	1.142593
81	1	-2.339995	-7.606171	2.023718
82	1	-1.566912	-8.861641	0.01908
83	6	-1.993254	-5.674518	1.14094
84	1	-2.329969	-5.131169	2.018948
85	6	-2.786127	-2.79282	0.015423
86	6	-4.062788	-3.471236	-0.045322
87	1	-4.198956	-4.54159	-0.084905
88	6	-5.018558	-2.50741	-0.058068
89	1	-6.089311	-2.63618	-0.109509
90	7	-2.965021	1.431099	-0.008507
91	7	-0.124946	1.428795	-0.024812
92	6	1.926235	2.50987	0.055174
93	1	2.997173	2.639526	0.10153
94	6	7.720825	0.000717	0.023069
95	6	8.444483	-0.328089	-1.138307
96	6	9.835075	-0.329194	-1.142644
97	1	10.373649	-0.593343	-2.04531
98	6	10.543774	-0.000523	0.022136
99	6	12.027016	0.01347	0.071895
100	8	12.686249	0.29595	1.058538
101	8	12.602216	-0.323725	-1.104135
102	1	13.56446	-0.285607	-0.969435
103	6	9.833872	0.328119	1.185576
104	1	10.386333	0.589792	2.081383
105	6	8.444721	0.328891	1.185198
106	1	7.912481	0.610237	2.087926
107	1	7.911584	-0.609263	-2.040683
108	1	6.042134	0.758615	-1.991816

Table S10. Energies (in hartree) for the optimized geometries provided in Tables S4-9

	B3LYP| 6-31G(d,p)	**B3LYP | TZVP**
TEMPO	- 483.750173	- 483.862334
TEMPOH	- 484.359752	- 484.473101
$Fe^{III}PhCO_2^-$	- 3816.774186	- 3817.676745
$Fe^{II}PhCO_2H$	- 3817.407030	- 3818.292971
$Fe^{III}Ph_2CO_2^-$	- 4047.838889	- 4048.805990
$Fe^{II}Ph_2CO_2H$	- 4049.422630	- 4048.472463

Table S11. Cartesian coordinates of the rigid portions of the iron-porphyrin molecules employed in calculation of $w_{\mathrm{r}}^{(1)}(R)$ and $w_{\mathrm{r}}^{(2)}(R)$.

$Fe^{III}PhCO_2^-$			
Atom Name	**X / Å**	**Y / Å**	**Z / Å**
C00	-0.07	13.20	-0.25
C01	-1.30	12.53	-0.24
C01	1.17	12.54	-0.27
C02	-2.57	13.20	-0.15
C02	2.44	13.22	-0.29
C03	-3.53	12.24	-0.15
C03	3.40	12.27	-0.30
C04	-2.86	10.97	-0.24
C04	2.74	10.99	-0.31
C05	-3.52	9.74	-0.24
C05	3.41	9.76	-0.33
C06	-5.02	9.73	-0.20
C06	4.91	9.76	-0.36
C07	-5.71	9.28	0.94
C07	-5.76	10.19	-1.30
C07	5.64	9.33	0.76
C07	5.60	10.20	-1.50
C08	-7.10	9.28	0.97
C08	-7.16	10.18	-1.27
C08	7.04	9.33	0.73
C08	7.00	10.20	-1.52
C09	-7.83	9.73	-0.13
C09	7.72	9.77	-0.41
C10	2.74	8.53	-0.33
C10	-2.85	8.51	-0.27
C11	3.42	7.26	-0.41
C11	-3.52	7.23	-0.30
C12	2.46	6.30	-0.42
C12	-2.55	6.28	-0.32
C13	1.18	6.97	-0.34
C13	-1.28	6.96	-0.33
C14	-0.05	6.31	-0.35
C15	-0.04	4.81	-0.39
C16	0.36	4.06	0.73
C16	-0.44	4.12	-1.55
C17	0.37	2.67	0.69

C17	-0.43	2.73	-1.59
C18	-0.03	2.00	-0.47
C24	-1.11	9.81	2.51
C24	1.00	9.70	-3.09
C25	0.65	9.72	3.85
C25	-0.76	9.79	-4.43
C26	1.06	9.69	2.55
C26	-1.17	9.81	-3.12
Fe	-0.10	9.75	-0.29
H01	-2.69	14.27	-0.09
H01	2.56	14.29	-0.29
H02	-4.60	12.37	-0.08
H02	4.47	12.40	-0.30
H03	-5.14	8.93	1.80
H03	-5.24	10.53	-2.19
H03	5.12	8.99	1.64
H03	5.04	10.54	-2.36
H04	-7.62	8.93	1.86
H04	-7.72	10.53	-2.13
H04	7.59	8.99	1.60
H04	7.52	10.54	-2.41
H05	-8.92	9.73	-0.11
H05	8.81	9.77	-0.43
H06	-4.59	7.09	-0.29
H06	4.49	7.13	-0.46
H07	-2.67	5.21	-0.33
H07	2.58	5.23	-0.48
H08	0.67	4.58	1.63
H08	-0.75	4.68	-2.42
H09	0.68	2.11	1.57
H09	-0.74	2.21	-2.49
H10	-0.02	0.91	-0.49
H13	-2.14	9.87	2.20
H13	2.03	9.64	-2.77
H14	-1.35	9.83	4.60
H14	1.24	9.69	-5.18
H15	1.19	9.69	4.78
H15	-1.30	9.83	-5.36
H16	2.06	9.64	2.16
H16	-2.17	9.87	-2.74
N01	1.37	11.17	-0.29

N01	-1.49	11.16	-0.28
N02	-1.48	8.33	-0.29
N02	1.38	8.34	-0.30
N03	-0.05	9.75	1.72
N03	-0.06	9.75	-2.30
N04	-0.73	9.79	3.80
N04	0.62	9.72	-4.38
$Fe^{III}Ph_2CO_2^-$			
Atom Name	**X / Å**	**Y / Å**	**Z / Å**
C00	-0.14	-35.72	-0.23
C01	-1.36	-35.05	-0.29
C01	1.10	-35.07	-0.22
C02	-2.63	-35.72	-0.41
C02	2.36	-35.76	-0.18
C03	-3.59	-34.75	-0.45
C03	3.34	-34.81	-0.22
C04	-2.92	-33.48	-0.35
C04	2.68	-33.53	-0.25
C05	-3.58	-32.25	-0.34
C05	3.35	-32.30	-0.29
C06	-5.07	-32.24	-0.38
C06	4.85	-32.31	-0.31
C07	-5.75	-31.74	-1.51
C07	-5.83	-32.72	0.70
C07	5.55	-31.92	-1.46
C07	5.59	-32.71	0.82
C08	-7.15	-31.73	-1.55
C08	-7.22	-32.71	0.65
C08	6.94	-31.92	-1.49
C08	6.98	-32.71	0.79
C09	-7.88	-32.21	-0.47
C09	7.66	-32.32	-0.36
C10	-2.90	-31.03	-0.26
C10	2.69	-31.07	-0.28
C11	3.37	-29.80	-0.23
C11	-3.56	-29.75	-0.17
C12	2.42	-28.84	-0.16
C12	-2.59	-28.80	-0.11
C13	1.14	-29.51	-0.19
C13	-1.32	-29.49	-0.14
C14	-0.09	-28.84	-0.12

C15	-0.07	-27.34	-0.20
C16	0.26	-26.55	-1.13
C16	-0.40	-26.71	1.19
C17	0.27	-25.16	-1.03
C17	-0.39	-25.31	1.28
C18	-0.05	-24.54	0.17
C24	-1.16	-32.09	-3.05
C24	0.95	-32.17	2.54
C25	0.57	-32.38	-4.40
C25	-0.79	-32.36	3.88
C26	0.98	-32.46	-3.10
C26	-1.21	-32.40	2.58
Fe	-0.11	-32.28	-0.26
H01	-2.76	-36.79	-0.46
H01	2.48	-36.83	-0.14
H02	-4.66	-34.88	-0.55
H02	4.41	-34.95	-0.22
H03	-5.18	-31.36	-2.35
H03	-5.31	-33.10	1.58
H03	4.99	-31.61	-2.34
H03	5.06	-33.01	1.72
H04	-7.65	-31.34	-2.43
H04	-7.79	-33.08	1.50
H04	7.47	-31.62	-2.39
H04	7.53	-33.02	1.68
H05	-8.97	-32.20	-0.50
H05	8.75	-32.32	-0.38
H06	-4.63	-29.60	-0.16
H06	4.44	-29.67	-0.22
H07	-2.70	-27.73	-0.44
H07	2.55	-27.77	-0.98
H08	0.51	-27.03	-2.07
H08	-0.66	-27.31	2.05
H09	0.53	-24.56	-1.90
H09	-0.64	-24.84	2.23
H10	-0.04	-23.45	0.25
H13	-2.17	-31.91	-2.74
H13	1.97	-32.06	2.22
H14	-1.40	-32.04	-5.14
H14	1.20	-32.15	4.62
H15	1.11	-32.47	-5.33

H15	-1.33	-32.42	4.81
H16	1.97	-32.63	-2.71
H16	-2.21	-32.51	2.20
N01	1.31	-33.70	-0.25
N01	-1.55	-33.68	-0.27
N02	-1.53	-30.85	-0.23
N02	1.33	-30.87	-0.26
N03	-0.11	-32.27	-2.26
N03	-0.11	-32.28	1.75
N04	-0.79	-32.15	-4.35
N04	0.58	-32.22	3.83

Table S12. Cartesian coordinates of the rigid portions of the iron-porphyrin molecules employed in calculation of $w_{\mathrm{p}}^{(1)}(R)$ and $w_{\mathrm{p}}^{(2)}(R)$.

$Fe^{II}PhCO_2H$			
Atom Name	**X / Å**	**Y / Å**	**Z / Å**
C00	-0.03	13.19	-0.34
C01	1.20	12.53	-0.34
C01	-1.28	12.54	-0.32
C02	2.48	13.20	-0.42
C02	-2.54	13.24	-0.30
C03	3.44	12.24	-0.43
C03	-3.51	12.29	-0.27
C04	2.75	10.97	-0.34
C04	-2.84	11.01	-0.26
C05	3.40	9.72	-0.35
C05	-3.51	9.78	-0.23
C06	4.90	9.71	-0.38
C06	-5.01	9.78	-0.20
C07	5.59	9.26	-1.52
C07	5.65	10.16	0.72
C07	-5.76	9.34	-1.30
C07	-5.71	10.23	0.94
C08	6.99	9.26	-1.55
C08	7.04	10.15	0.69
C08	-7.16	9.35	-1.27
C08	-7.10	10.24	0.97
C09	7.72	9.70	-0.44
C09	-7.83	9.80	-0.14
C10	-2.86	8.53	-0.24
C10	2.73	8.49	-0.32
C11	-3.55	7.26	-0.16
C11	3.40	7.21	-0.30
C12	-2.59	6.30	-0.16
C12	2.43	6.26	-0.28
C13	-1.31	6.98	-0.24
C13	1.16	6.96	-0.27
C14	-0.08	6.31	-0.24
C15	-0.09	4.81	-0.21
C16	-0.52	4.07	-1.33
C16	0.32	4.11	0.93
C17	-0.53	2.68	-1.31

C17	0.31	2.71	0.96
C18	-0.12	1.99	-0.16
C24	0.99	9.75	-3.11
C24	-1.11	9.75	2.53
C25	-0.76	9.75	-4.45
C25	0.65	9.75	3.87
C26	-1.17	9.75	-3.15
C26	1.06	9.75	2.57
Fe	-0.10	9.75	-0.29
H01	2.62	14.27	-0.48
H01	-2.67	14.31	-0.30
H02	4.51	12.36	-0.49
H02	-4.58	12.43	-0.26
H03	5.03	8.92	-2.38
H03	5.13	10.51	1.61
H03	-5.24	9.00	-2.19
H03	-5.14	10.57	1.80
H04	7.50	8.91	-2.44
H04	7.60	10.50	1.56
H04	-7.71	9.01	-2.14
H04	-7.62	10.59	1.86
H05	8.80	9.69	-0.47
H05	-8.92	9.80	-0.11
H06	4.47	7.06	-0.31
H06	-4.62	7.14	-0.09
H07	2.55	5.19	-0.27
H07	-2.73	5.23	-0.10
H08	-0.84	4.60	-2.22
H08	0.65	4.66	1.80
H09	-0.86	2.13	-2.18
H09	0.63	2.19	1.85
H10	-0.13	0.90	-0.14
H13	2.02	9.75	-2.79
H13	-2.14	9.75	2.21
H14	1.24	9.75	-5.21
H14	-1.35	9.75	4.63
H15	-1.31	9.75	-5.38
H15	1.20	9.76	4.80
H16	-2.17	9.75	-2.75
H16	2.06	9.75	2.17
N01	-1.47	11.18	-0.29

N01	1.38	11.16	-0.30
N02	1.36	8.32	-0.29
N02	-1.50	8.34	-0.28
N03	-0.07	9.75	-2.31
N03	-0.05	9.75	1.73
N04	0.61	9.75	-4.41
N04	-0.73	9.75	3.83
$Fe^{II}Ph_2CO_2H$			
Atom Name	**X / Å**	**Y / Å**	**Z / Å**
C00	0.01	-35.72	-0.22
C01	1.23	-35.02	-0.22
C01	-1.25	-35.10	-0.23
C02	2.52	-35.66	-0.14
C02	-2.50	-35.84	-0.24
C03	3.45	-34.67	-0.14
C03	-3.50	-34.91	-0.25
C04	2.73	-33.41	-0.22
C04	-2.86	-33.61	-0.27
C05	3.34	-32.15	-0.21
C05	-3.57	-32.40	-0.29
C06	4.84	-32.10	-0.19
C06	-5.07	-32.45	-0.31
C07	5.53	-31.63	0.95
C07	5.60	-32.53	-1.29
C07	-5.81	-32.03	0.80
C07	-5.76	-32.92	-1.44
C08	6.92	-31.58	0.97
C08	6.99	-32.48	-1.27
C08	-7.21	-32.07	0.78
C08	-7.15	-32.97	-1.46
C09	7.66	-32.01	-0.13
C09	-7.88	-32.54	-0.35
C10	2.64	-30.94	-0.24
C10	-2.95	-31.14	-0.29
C11	-3.67	-29.89	-0.37
C11	3.27	-29.64	-0.26
C12	-2.74	-28.90	-0.38
C12	2.28	-28.72	-0.28
C13	-1.45	-29.54	-0.30
C13	1.03	-29.45	-0.29
C14	-0.23	-28.84	-0.31

C15	-0.29	-27.34	-0.35
C16	-0.73	-26.61	0.77
C16	0.10	-26.63	-1.50
C17	-0.78	-25.21	0.73
C17	0.05	-25.24	-1.53
C18	-0.39	-24.52	-0.42
C24	0.95	-32.24	2.56
C24	-1.17	-32.31	-3.07
C25	-0.80	-32.30	3.91
C25	0.58	-32.26	-4.42
C26	-1.21	-32.31	2.61
C26	0.99	-32.24	-3.12
Fe	-0.11	-32.28	-0.26
H01	2.69	-36.72	-0.09
H01	-2.59	-36.91	-0.24
H02	4.52	-34.76	-0.08
H02	-4.56	-35.09	-0.25
H03	4.96	-31.30	1.81
H03	5.08	-32.89	-2.18
H03	-5.30	-31.67	1.68
H03	-5.19	-33.25	-2.31
H04	7.43	-31.22	1.86
H04	7.56	-32.81	-2.13
H04	-7.77	-31.75	1.66
H04	-7.67	-33.33	-2.34
H05	8.75	-31.97	-0.11
H05	-8.97	-32.58	-0.36
H06	4.34	-29.47	-0.25
H06	-4.75	-29.79	-0.43
H07	2.37	-27.64	-0.29
H07	-2.91	-27.83	-0.44
H08	-1.03	-27.14	1.66
H08	0.44	-27.18	-2.37
H09	-1.13	-24.67	1.61
H09	0.35	-24.71	-2.43
H10	-0.43	-23.44	-0.44
H13	1.98	-32.21	2.24
H13	-2.20	-32.34	-2.75
H14	1.20	-32.23	4.65
H14	-1.43	-32.32	-5.17
H15	-1.34	-32.32	4.84

H15	1.12	-32.24	-5.36
H16	-2.22	-32.35	2.22
H16	1.99	-32.21	-2.73
N01	-1.49	-33.75	-0.25
N01	1.37	-33.65	-0.25
N02	1.27	-30.81	-0.26
N02	-1.59	-30.91	-0.26
N03	-0.11	-32.28	1.77
N03	-0.11	-32.28	-2.28
N04	0.58	-32.25	3.86
N04	-0.80	-32.30	-4.38